INTERACTION OF ATP AND ALPHA-SYNUCLEIN

INVESTIGATING THE INTERACTION MECHANISM AND EFFECT OF ATP ON ALPHA-SYNUCLEIN AGGREGATION BY NMR SPECTROSCOPY

By EVELYN ROSE KAMSKI-HENNEKAM, B.Sc.

A Thesis Submitted to the School of Graduate Studies in Partial Fulfilment of the Requirement for the Degree Master of Science

McMaster University MASTER OF SCIENCE (2022) Hamilton, ON (Chemical Biology)

TITLE: Investigating the Interaction Mechanism and Effect of ATP on Alpha-Synuclein Aggregation by NMR Spectroscopy

AUTHOR: Evelyn Rose Kamski-Hennekam, B.Sc. (University of Guelph, Guelph, ON)

SUPERVISOR: Professor Giuseppe Melacini

NUMBER OF PAGES: xiv, 100

Lay Abstract

Alpha-synuclein (αS) is a protein whose abnormal aggregation is characteristic of Parkinson's Disease (PD). Adenosine Triphosphate (ATP) is a molecule that has recently been shown to reduce the aggregation of select disease-causing proteins. Therefore, the aim of this study is to characterize the interaction mechanism between ATP and αS, to explore how this interaction influences αS structural dynamics and to determine the effect of ATP on early- and late-stage αS aggregation. Another overall aim of this study is to characterize how the ATP-αS interaction is influenced by PD-related mutations in αS. To accomplish these aims, we will rely primarily on NMR spectroscopy as well as fluorescence and microscopy techniques. Our goal is to determine the role of ATP in αS aggregation as well as potentially connect the age-related decrease in ATP levels with PD, an age-related disease.

Abstract

Recent studies suggest that Adenosine Triphosphate (ATP) can either enhance or inhibit the aggregation of amyloid proteins, depending on the interaction mechanism as well as specific protein properties. The connection between ATP and protein solubility is particularly important in Parkinson's Disease (PD), where the aggregation of alpha-synuclein (αS) is closely linked to pathology. Since the greatest risk factor for PD is aging, and ATP levels decline dramatically with age and are greatly reduced in the brains of patients with early PD, it is possible that the modulating effect of ATP on protein solubility is a factor in PD onset. However, the driving mechanism behind the interaction of ATP and αS is currently unclear, as is the effect of physiologically-relevant ATP concentrations on early- and late-stage αS aggregation. Here, we determine using NMR spectroscopy that the triphosphate moeity of ATP drives its electrostatic interaction primarily with the N-terminal pseudo-apolipoprotein repeats of αS monomers. These interactions are modulated by magnesium and disrupt long-range N- to C-terminal contacts in αS monomers, causing a concentration-dependent enhancement of initial αS aggregation. We also show by Thioflavin T fluorescence as well as electron microscopy that ATP inhibits late-stage αS β-sheet fibril formation in a phosphate-dependent manner. Our NMR data reveals that ATP inhibits αS monomer-fibril interactions, suggesting that ATP attenuates αS secondary nucleation. Lastly, we show that the effects of ATP are different in the presence of PD-related αS mutations E46K and A53T. Overall, our study contributes a thorough characterization of the biologically- and pathologically-relevant interactions between ATP and αS, while also proposing a role for ATP in the age-related development of PD pathology.

Acknowledgements

First, I would like to express my sincere gratitude to my graduate thesis supervisor, Dr. Giuseppe Melacini, for accepting me into his lab group and for his support throughout my graduate studies. Without his detailed explanations of NMR pulse-sequences, his willingness to schedule personal help sessions at the spectrometer, and his dedication to answering my numerous questions, I would have struggled much more in my understanding and application of NMR experiments. In addition, Dr. Melacini's detailed feedback on presentations and data analysis, as well as his encouragement that I attend conferences and symposia, greatly enriched my graduate experience.

Secondly, I would like to thank my committee members, Dr. José Moran-Mirabal and Dr. Maikel C. Rheinstädter, for their kindness and enthusiastic support during my committee meetings. I also greatly appreciate their willingness to personally aid my project by applying their expertise in fluorescence microscopy and MD simulations.

I also cannot express enough my thanks to members of the Melacini lab for creating a supportive and welcoming environment for me to work in. In particular, I would like to thank Dr. Rashik Ahmed and Jinfeng Huang, who started the alpha-synuclein project in the Melacini lab and taught me the relevant protocols with great patience and generous support. In addition, I would like to thank Dr. Madoka Akimoto, Karla Martinez Pomier, Qiulin Ma, Hebatallah Mohamed and Mariia Khamina for their help and encouragement.

Lastly, I would like to thank Dr. Bob Berno and Dr. Hilary Jenkins of the McMaster NMR facility, as well as the staff at the Biointerfaces Institute and the Canadian Centre for Electron Microscopy, for their valuable support in completing my project.

Table of Contents

Chapter 2

Chapter 3

List of Figures and Tables

List of Abbreviations and Symbols

αS	Alpha-Synuclein
WT	Wild-Type
PD	Parkinson’s Disease
EGCG (-)-	Epigallocatechin Gallate
NAC	Non-amyloid-β Component
Mg^{2+}	Magnesium Ion
ThT	Thioflavin T
ATP	Adenosine Triphosphate
ATP-Mg	ATP Complexed with Mg^{2+}
LLPS	Liquid-Liquid Phase Separation
FUS	Fused-In-Sarcoma Protein
ADP	Adenosine Diphosphate
HMW	High-Molecular-Weight
hIAPP	Human Islet Amyloid Polypeptide
AcP	Human Muscle Acylphosphatase
AMP	Adenosine Monophosphate
NMR	Nuclear Magnetic Resonance Spectroscopy
STD	Saturation Transfer Difference
DLS	Dynamic Light Scattering
TEM	Transmission Electron Microscopy
IPTG	Isopropyl β-D-1-Thiogalactopyranoside
HSQC	Heteronuclear Single Quantum Coherence

K_d	Dissociation Constant
CHESPA	CHEmical Shift Projection Analysis
PRE	Paramagnetic Relaxation Enhancement
STR	Saturation Transfer Reference
SEC-MALS	Size Exclusion Chromatography Coupled with Multiangle Light Scattering
SDS-PAGE	Sodium Dodecyl-Sulfate Polyacrylamide Gel Electrophoresis
LMW	Low-Molecular-Weight
IMW	Intermediate-Molecular-Weight
CD	Circular Dichroism Spectroscopy
FRAP	Fluorescence Recovery After Photobleaching
Δ	Delta
Γ	Tau
Θ	Theta

Declaration of Academic Achievement

The majority of experimental work was done by author Evelyn Rose Kamski-Hennekam, although the setup of some ThT experiments and DLS measurements was done by Dr. Rashik Ahmed and Jinfeng Huang. The thesis content was written by author Evelyn Rose Kamski-Hennekam and was co-edited by Evelyn Rose Kamski-Hennekam and Dr. Giuseppe Melacini, who also assisted with the setup of some NMR experiments.

Chapter 1

Introduction to Alpha-Synuclein and ATP

1.1 Alpha-Synuclein: Its Function, Sequence and Structure

Alpha-synuclein (αS) is a 140-amino-acid-long protein (Figure 1a) that is expressed throughout the human body, including in the heart and muscle tissue, the peripheral and enteric nervous systems, the liver, lungs and kidneys, as well as in bone marrow and in circulating blood cells (Alza *et al.,* 2019; Moons *et al.,* 2020). However, its levels are highest at 5 - 50 µM in primarily the cytosol of pre-synaptic nerve termini in the central nervous system, specifically in certain brain regions including the neocortex, hippocampus, SN, thalamus, and cerebellum (Alza *et al.,* 2019; Bisi *et al.,* 2021; Moons *et al.,* 2020; Sawada *et al.,* 2020). As such, it is believed to function mainly in synaptic vesicle trafficking by selectively binding lipid membranes, although it has also been shown to modulate neurotransmitter release through SNARE complex assembly and disassembly, regulate the expression of genes involved in dopamine synthesis and protect neurons under oxidative stress conditions as well as modulate mitophagy, exo- and endocytosis and lipid/fatty acid metabolism (Bozelli Jr. *et al.,* 2021; Dettmer *et al.,* 2015; Prahl *et al.,* 2022; Ramis *et al.,* 2020). Recent studies have also suggested that the normal, physiological function of αS involves regulating cell proliferation and differentiation as well as inducing inflammatory and immune responses, since αS knockout mice are particularly suspectable to viral infections and are significantly deficient in leukocyte recruitment in response to inflammatory stimuli (Alam *et al.,* 2022; Prahl *et*

al., 2022). With so many different functions reported, the main biological role of αS remains unclear and controversial.

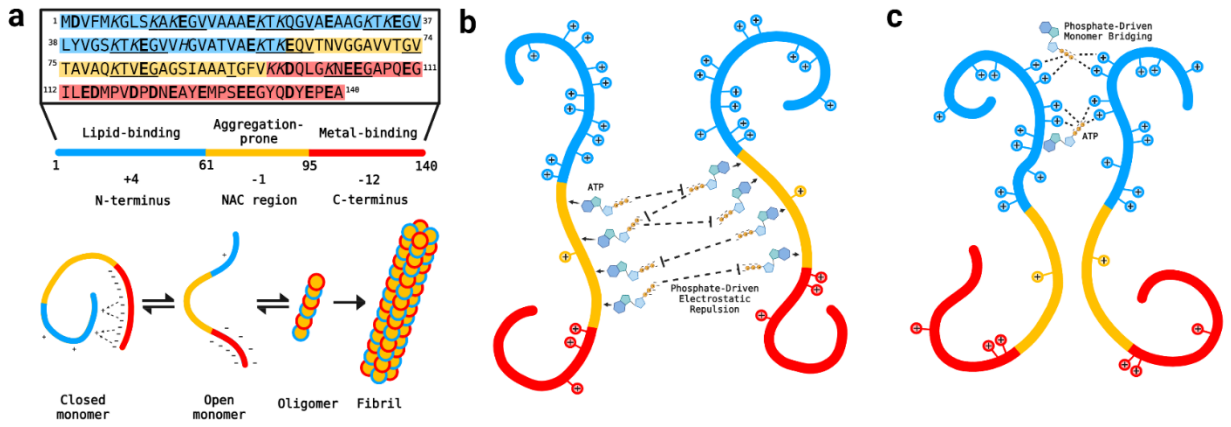

Figure 1. Hypothetical models of αS-ATP interactions. (a) Schematic showing the sequence of wild-type (WT) αS, which contains nine total pseudo-apolipoprotein-like repeats (underlined), as well as different proportions of acidic (bolded) and basic (italicized) residues. The sequence is colored according to three principal regions: the N-terminus (blue), responsible for lipid binding, the aggregation-prone Non-Amyloid-β component (NAC) region (yellow) and the C-terminus (red), which contains metal-binding sites. Shown below is a general mechanism of αS aggregation, whereby disruption of the long-range electrostatic contacts between the N- and C-termini of closed αS monomers leads to opening and subsequent aggregation of αS into oligomers and fibrils. (b) One hypothetical model showing a possible interaction mechanism between ATP and αS. Based upon published models for the interaction of ATP with other proteins, *e.g.,* in the crystalline lens, it is possible that ATP acts to inhibit αS monomer association and subsequent aggregation by clustering over the hydrophobic, aggregation-prone NAC region of αS and electrostatically repelling other bound monomers via the exposed triphosphate moiety (Greiner and Glonek, 2020). (c) Another viable model for the ATP-αS interaction suggests that ATP could bridge αS monomers and enhance aggregation via the phosphate-mediated targeting of lysine residues in the αS N-terminus, as is the case for Tau protein (Heo *et al.,* 2020). Figure prepared in Biorender.

αS monomers can be divided into three main regions, each with unique physico-chemical properties conferred by a distinct amino acid composition (Figure 1a) (Bisi *et al.,* 2021). Residues 1 – 60 constitute the N-terminus, which is particularly rich in lysine residues and has an overall positive charge (Figure 1a) (Kumari *et al.,* 2021). This region contains amphipathic repeats of 11 amino acids, which themselves contain the highly conserved, consensus sequence "KTKEGV" (Figure 1a) (Alza *et al.,* 2019; Bisi *et al.,* 2021). These repeats are present nine times either completely or partially in the αS sequence (Figure 1a) and are similar to those present in apolipoprotein domains; thus, they confer lipid-binding properties to αS (Alza *et al.,* 2019). Upon binding to negatively-charged membranes or vesicles, the N-terminal region of αS monomers adopts an α-helical structure that can also involve the central non-amyloid β component, or NAC region (Alza *et al.,* 2019; Bozelli Jr. *et al.,* 2021; Moons *et al.,* 2020). The latter is composed of residues 61 – 95, is predominantly hydrophobic and is responsible for sensing membrane properties (Figure 1a) (Bozelli Jr. *et al.,* 2021; Ramis *et al.,* 2020). In addition, the NAC region plays a critical role in abnormal αS aggregation by driving the conformational change of αS monomers from predominantly random-coil to β-sheet, a change which leads to amyloid fibril formation and stabilizes fibrils (Alza *et al.,* 2019; Prahl *et al.,* 2022; Ramis *et al.,* 2020). Finally, the disordered C-terminus of αS monomers comprises residues 96 – 140 and is enriched in glutamate, aspartate, and proline residues and is therefore highly acidic, with an overall negative charge (Figure 1a) (Alza *et al.,* 2019; Prahl *et al.,* 2022). As such, this region is essential for binding a variety of metal ions (Figure 1a), although it also drives the interaction between αS and other proteins, has chaperone-like activity and is the main site of post-translational modifications,

including phosphorylation and nitration as well as truncations (Alza *et al.,* 2019; Bozelli Jr. *et al.,* 2021; Moons *et al.,* 2020; Prahl *et al.,* 2022). With such different chemical properties, the three regions of αS can also interact with each other, and it is modulations of these intramolecular interactions which drive changes in αS structure (Figure 1a) (Moons *et al.,* 2020).

The overall conformation of αS monomers in solution is a matter of intense debate. Wild-type (WT) αS monomers do not adopt a single, equilibrium structure under physiological conditions, but rather exist in a dynamic ensemble of conformations that have led to αS being classified as a structurally heterogeneous, Intrinsically Disordered Protein, or IDP (Bisi *et al.,* 2021). Since αS is a natively unfolded protein lacking a well-defined 3D structure, there is great controversy around whether or not αS monomers in solution adopt a compact, globular-like structure or exist as an extended random coil (Bisi *et al.,* 2021; Ramis *et al.,* 2020). The general consensus is that cytosolic αS is monomeric, although recent research from multiple groups suggests that αS also forms α-helical tetramers in solution and could also form a small number of isolated β-sheets (Bisi *et al.,* 2021; Bozelli Jr. *et al.,* 2021; Dettmer *et al.,* 2015). This “multimerization” of αS in solution arises most likely from the conserved “KTKEGV” repeats, as single-point substitutions within this sequence, particularly of the threonine, glutamic acid and glycine residues completely abolish tetramer and associated multimer formation (Dettmer *et al.,* 2015). Importantly, these tetramers likely mediate αS-induced cytotoxicity, as multimer-abolishing mutations in the “KTKEGV” motifs lead to neuronal death as well as an increased presence of insoluble αS in cytoplasmic inclusions (Dettmer *et al.,* 2015). The tetramers therefore likely represent an auto-inhibitory mechanism of αS to prevent the

abnormal formation of cytotoxic inclusions, an effect which is similar to that of long-range electrostatic contacts between the N- and C-termini of αS monomers (Figure 1a) (Bisi *et al.,* 2021; Dettmer *et al.,* 2015). These contacts, though transient, serve to shield the aggregation-prone NAC region and thereby inhibit αS fibrillization by stabilizing non-aggregative conformations (Figure 1a) (Ramis *et al.,* 2020). Consequently, perturbation of these contacts leads to exposure of the hydrophobic NAC region, allowing it to establish intermolecular interactions that drive oligomer and fibril formation (Figure 1a) (Bisi *et al.,* 2021). Thus, although αS monomers are classified as unfolded, changes in overall monomer conformation and intermolecular contacts have important impacts on structure and therefore, function (Bisi *et al.,* 2021).

1.2 αS Aggregation and Parkinson's Disease

As aforementioned, αS can form insoluble, cytotoxic, β-sheet-rich amyloid fibrils, and these characterize a spectrum of neurodegenerative diseases called synucleinopathies which include Parkinson's Disease (PD), Lewy body-related dementia and Alzheimer's Disease, Krabbe disease, neurodegeneration with brain iron accumulation and Multiple System Atrophy (Alza *et al.,* 2019; Hoyer *et al.,* 2002). PD in particular is defined neuropathologically by cytoplasmic intraneuronal inclusions called Lewy bodies and Lewy neurites, of which aggregated or fibrillar αS is the major structural component (Hoyer *et al.,* 2002; Sawada *et al.,* 2020). This connection between αS and PD is further supported by the fact that genetic mutations associated with familial PD occur exclusively in the αS *SNCA* gene, elevated αS levels due to *SNCA* gene duplication and triplication lead to early-onset PD, sporadic forms of PD also cause αS accumulation

and transgenic animal models of mice and Drosophila over-expressing human αS develop PD-like symptoms, including motor deficits and cytoplasmic, Lewy-body-like inclusions rich in αS (Ahmed *et al.,* 2020; Alza *et al.,* 2019; Hoyer *et al.,* 2002; Kumari *et al.,* 2021). Thus, the aggregation of αS has been implicated as an important factor in PD development, although whether or not it is the pathological cause remains complex and controversial (Ahmed *et al.,* 2020).

Nonetheless, the significant connection between αS aggregation and disease has led to intense research into the aggregation pathway of αS. As stated earlier, αS monomers can undergo structural transitions, from random-coil or α-helical conformations to pathological β-sheets, that accelerate their assembly into large, insoluble aggregates that are toxic to cells (Alza *et al.,* 2019; Moons *et al.,* 2020). This aggregation mechanism is complex and proceeds most likely through a nucleation-dependent polymerization reaction, beginning with the slow formation of primary nuclei formed by αS monomers adopting a β-sheet structure similar to that present in mature fibrils (de Oliveira and Silva, 2019; Kumari *et al.,* 2021). The fusion of small β-sheet species into the minimum template required for self-assembly is the rate-limiting step (de Oliveira and Silva, 2019). Therefore, it can be accelerated by the local concentration of αS monomers at air-water interfaces as well as lipid membrane surfaces, causing supersaturation (de Oliveira and Silva, 2019; Furukawa *et al.,* 2020). Another model of αS aggregation postulates that αS monomers collapse via inter-molecular interactions and form disordered oligomers that slowly change into aggregation-competent, β-sheet-rich species (de Oliveira and Silva, 2019). The formation of β-sheet-rich αS oligomeric intermediates, representing the primary neurotoxic species that contribute to PD-associated neurodegeneration, then

leads to protofibril and eventually full-length fibril formation either as single monomer units add to and elongate fibril ends or via the assembly of multiple protofilaments (Ahmed *et al.,* 2020; Chen *et al.,* 2015; Kumari *et al.,* 2021). Mature amyloid fibrils exhibit a characteristic cross-β-sheet structure involving β-strands aligned perpendicularly to the fibril axis and β-sheets oriented parallel to the fibril axis (Chen *et al.,* 2015). These αS fibrils can also multiply by fragmentation, which creates a greater number of "active" fibril ends to serve as primary nuclei and thereby accelerates aggregation, or via a process known as secondary nucleation (Furukawa *et al.,* 2020; Kumari *et al.,* 2021). The latter process is believed to dominate under physiologically-relevant quiescent conditions and is particularly pathologically important in that it dramatically accelerates αS aggregation, especially at low pH (Buell *et al.,* 2014). As such, an active area of therapeutically-relevant research involves attempting to inhibit such transient αS monomer-fibril interactions, since these are likely important for spreading PD pathology (Kumari *et al.,* 2021).

Secondary nucleation of αS is able to accelerate the conversion of monomers into aggregates both by artificially concentrating monomers and by causing unfolding of partially collapsed, disordered monomers into more open, aggregation-prone states via fibril binding (Kumari *et al.,* 2021). This binding is driven primarily by the N-terminal 40 residues of αS monomers, with residues 1 to 20 having particularly significant increases in R_2 transverse ^{15}N amide relaxation parameters to indicate increased on-off chemical exchange dynamics (Kumari *et al.,* 2021). Furthermore, this interaction has a highly significant electrostatic component and is attenuated in the presence of fibrils formed by C-terminally-truncated αS monomers, suggesting that the positively-charged N-terminus of monomers binds to the exposed, highly negatively-charged C-terminus of fibril-

incorporated monomers (Kumari *et al.,* 2021). Nonetheless, Kumari *et al.,* (2021) also show that aromatic π–π interactions are critically important for transient αS monomer-fibril interactions. Such interactions also favor more extended αS monomer conformations and thereby compete with long-range, electrostatic contacts between the N- and C-termini of αS monomers in solution (Kumari *et al.,* 2021). Recruitment of "free" monomers to the fibril surface via secondary nucleation has also been shown to initiate seeding of αS aggregation, highlighting the fact that these monomer-fibril interactions are important for the "prion-like" spread of PD pathology (Kumari *et al.,* 2021).

αS oligomers, which are released by unconventional exocytosis from "PD-affected" cells, show an enhanced ability to enter recipient cells and thereby spread toxic PD pathology to drive neurodegeneration (Ahmed *et al.,* 2020). This "prion-like" ability of αS oligomers is particularly relevant to the Braak hypothesis, which postulates that sporadic PD is initiated in the neurons of both the nasal cavity and the gut (Rietdijk *et al.,* 2017). From there, aggregated αS species spread via the vagus nerve and olfactory bulb to the central nervous system and eventually neurons of the substantia nigra, where characteristic PD-related neuron loss occurs (Rietdijk *et al.,* 2017). Importantly, αS oligomers have been detected in blood plasma and cerebrospinal fluid, suggesting that they likely play a key role in the spread of PD pathology according to the Braak hypothesis (Ahmed *et al.,* 2020; Rietdijk *et al.,* 2017). Coupled to their characterization as the primary neurotoxic species of αS aggregates, this makes oligomers, and any interactions involving them, vitally important therapeutic targets (Fusco *et al.,* 2017). Interestingly, the toxicity of αS oligomers is correlated with structural differences (Fusco *et al.,* 2017). Toxic oligomers, capable of significantly compromising lipid bilayers, inducing substantial

increases in reactive oxygen species and reducing mitochondrial activity, have a significantly higher β-sheet content than non-toxic oligomers (Fusco *et al.,* 2017). As well, they have highly mobile and accessible N- and C-termini, with the first 25 N-terminal residues promoting the strong, toxic membrane interaction (Fusco *et al.,* 2017). Given this significant connection between αS oligomer structure and toxicity, it is interesting to speculate whether therapeutic strategies could be developed that remodel oligomer structures from toxic to non-toxic forms, similar to the remodeling of aβ oligomers by (-)-Epigallocatechin gallate (EGCG) (Ahmed *et al.,* 2017).

The link between αS structure and toxicity is even more complex following the conversion of oligomers into mature fibrils, as at least 24 different fibril conformations with different templating regions and protofibril interfaces have been reported, along with many distinct disease pathologies (Holec *et al.,* 2022). This diversity in neurological disorders all linked to αS aggregation has given rise to the "strain hypothesis," which postulates that the specific synucleinopathy a patient develops is a direct result of which fibril conformation they have (Holec *et al.,* 2022). Although the αS residues involved in the fibril core differ slightly between conformations, generally the WT fibril core begins around residue 38 and comprises up to approximately residue 97 and involves parallel β-strands while the residues N-terminal to 38 and C-terminal to 97 remain disordered (Cho *et al.,* 2011). Within the core, residues T44-G47 form a loop separating two β-strands formed by residues L38-K43 and V48-N65, while the remaining residues up to 97 form regions with alternating levels of solvent exposure, V70-Q79 being the most protected (Cho *et al.,* 2011). Importantly, this core appears unaffected by the PD-related A30P mutation, while the A53T mutation creates an extended core region involving residues 30 – 100 (Cho *et*

al., 2011). It is possible that the differences in αS fibril structure between the WT and A53T variants are related to the increased aggregation propensity of A53T αS, although detailed studies linking specific αS fibril conformations to distinct disease symptoms in animal models are lacking (Cho *et al.,* 2011). This is true too for the E46K αS PD variant, although a detailed structural study by Boyer *et al.* (2020) recently established that the increased seeding potential of E46K fibrils compared to WT likely results from an increased monomer-fibril charge-driven attraction, which the authors attribute to the doubled number of electrostatic triads in the mutant fibrils. Furthermore, Boyer *et al.* (2020) hypothesize that the significantly greater reduction in mitochondrial activity by E46K versus WT fibrils that they observe is due to altered fibril surfaces (Boyer *et al.,* 2020). However, they do not provide a detailed characterization of how the differing protofilament folds and interfaces drive pathology (Boyer *et al.,* 2020). Nevertheless, the profound effect of a single amino acid change on αS fibrillization kinetics highlights the importance of even relatively minor changes to αS cytotoxicity and disease propensity (Cho *et al.,* 2011).

1.3 Factors Affecting αS Aggregation

Given the connection between αS aggregation and PD, factors that either enhance or inhibit pathologically-relevant αS aggregation are subjects of intense research and therapeutic interest. Charged species, both positive and negative, as well as changes in buffer pH and ionic strength have particularly potent affects on αS aggregation, likely by disrupting the long-range electrostatic contacts that provide the basis for the auto-inhibition of αS aggregation (Cohlberg *et al.,* 2002; Hoyer *et al.,* 2004). Interestingly, both

negatively- and positively-charged species enhance αS aggregation: heparin, a negatively-charged glycosaminoglycan, reduces the lag time of WT αS aggregation 6-fold from 17.8 to 2.9 hrs, while positively-charged polyamines like spermine significantly decrease the aggregation half-time of αS in a concentration-dependent manner (Cohlberg *et al.,* 2002; Hoyer *et al.,* 2004). The latter effect is due to spermine binding to residues 109-140 of αS monomers and shielding or reducing the net negative charge of the C-terminus, thereby reducing its ability to inhibit the self-aggregation of the amyloidogenic NAC region (Hoyer *et al.,* 2004). Consistent with this effect is that of Na^+, which also specifically binds residues 109-140 with a high affinity albeit with a lower overall binding capacity (Hoyer *et al.,* 2004). Na^+ enhances the average radius of gyration and solvent-accessibility of αS monomers at intermediate NaCl concentrations less than 0.1M, thereby favoring an extended and particularly aggregation-prone monomer conformation (Moons *et al.,* 2020; Ramis *et al.,* 2020). However, at high concentrations between 0.1 and 1M, NaCl actually has an opposite effect, whereby the C-terminal domain of αS monomers interacts less preferentially with Na^+ ions and is therefore less effectively charge-neutralized (Ramis *et al.,* 2020). This strengthens particularly the transient, long-range N- to C-terminal contacts in αS monomers, causing decreased solvent accessibility and likely yielding either amorphous aggregates by preventing the completion of fibrillization or inducing the formation of predominantly short fibrils (Ramis *et al.,* 2020). Clearly then, additives can affect not only αS aggregation kinetics but also the morphology of the aggregates themselves.

One additive with such an effect is Magnesium (Mg^{2+}), which binds at and above a protein: metal ratio of 1: 4 to mainly carboxylate side-chains in aspartic and glutamic

acid residues within the C-terminus of αS monomers, specifically in residues 109 – 140 (Hoyer *et al.,* 2004; Moons *et al.,* 2020). Although its binding affinity to αS is relatively low, up to eight Mg^{2+} ions can be coordinated by one αS monomer (Moons *et al.,* 2020). Interestingly, the binding of Mg^{2+} to αS monomers affects primarily tertiary but not secondary structure and causes monomer compaction likely by Mg^{2+} affecting the charge distribution along the protein surface and causing long-range structural reorganization (Hoyer *et al.,* 2004; Moons *et al.,* 2020). The effect of these changes on αS aggregation, however, is far from clear. Hoyer *et al.* (2004) report that 10 mM Mg^{2+} enhances aggregation of WT, A30P and A53T αS by inhibiting the shielding of the amyloidogenic NAC region by the bound and compacted C-terminus, while Golts *et al.* (2002) report that Mg^{2+} concentrations above 0.75 mM inhibit either spontaneous or iron-induced aggregation of WT, but not A53T, αS. Thus, the general consensus is that Mg^{2+} affects αS aggregation kinetics, but whether that effect is inhibitory or enhancing is still unclear. In addition, whether or not the proposed enhancing effect of 10 mM Mg^{2+} on αS aggregation leads to the formation of large fibril assemblies or amorphous aggregates containing densely-packed smaller fibrils is debatable, as both results have been reported (Hoyer *et al.,* 2002; Hoyer *et al.,* 2004). Nevertheless, since Mg^{2+} concentrations in cells are estimated at approximately 0.5 mM on average, it is likely that the binding of Mg^{2+} to αS is physiologically-significant and therefore could affect protein aggregation and morphology (Golts *et al.,* 2002).

Another factor which profoundly influences both the aggregation kinetics and fibril structure of αS is single amino-acid substitutions of the WT sequence, many of which have been linked to familial, early-onset cases of PD and most of which occur in the αS

N-terminal region (Stephens *et al.,* 2020). In particular, the A53T and E46K mutations are the hallmark of hereditary autosomal dominant PD and dramatically increase αS aggregation by shortening the lag time (Stephens *et al.,* 2020). Interestingly, the differences between mutant and WT αS are more significant for the E46K variant, which exhibits increased long-range electrostatic contacts between the N- and C-termini of monomers and causes a significantly altered protofibril interface (Bisi *et al.,* 2021; Holec *et al.,* 2022). The latter results in increased flexibility of the N-terminal region of the fibril core, lower fibril stability and looser fibril packing, all factors which could increase fragmentation and result in the observed enhancement of ThT-monitored aggregation (Holec *et al.,* 2022). By contrast, the shortened lag time and dramatically increased plateau ThT fluorescence for A53T αS relative to WT could be due to the significant solvent-deprotection at the N-terminus of A53T αS, reported by Stephens *et al.* (2020), which likely reflects local unfolding and the breaking of hydrogen bonds that stabilize αS monomers against aggregation. By contrast, multiple other research groups have reported no significant differences in monomer secondary structure or long-range N- to C-terminal electrostatic contacts between the A53T αS variant and WT (Bisi *et al.,* 2021). In addition, the fibril structures solved thus far for A53T αS indicate that the overall filament structure is similar to WT, with some alterations in protofilament interactions causing a shorter protofilament interface and less stable fibrils (Holec *et al.,* 2022). As such, it is possible that the significant, pathological effect of the A53T αS mutation may be related instead to altered protein interactions or the increased effect of a biological additive, as spermine dramatically enhances A53T aggregation relative to WT (Hoyer *et al.,* 2004). Additionally, de Oliveira and Silva (2019) show that although the fibrillar end-

products of WT and A53T αS aggregation are similar, the two variants have different populations of small oligomers, large oligomers and multimers during the early stages of aggregation, suggesting perhaps that WT and A53T αS have different aggregation pathways involving distinct intermediate species which cause the altered fibrillization kinetics. The different relative populations of oligomers between WT and A53T αS also create the possibility of distinct effects from oligomer-targeting chaperones such as Hsp90, which binds exclusively to A53T oligomers over monomers and fibrils and abolishes their toxicity to SHSY5Y neuroblastoma cells while inhibiting overall aggregation (Daturpalli *et al.,* 2013). Thus, interactions involving αS oligomers represent key aggregation checkpoints with enormous therapeutic potential.

Polyphosphates are particularly interesting enhancers of αS aggregation since they interact primarily with nucleation-competent oligomers over monomers and significantly alter fibril morphology to reduce cytotoxicity (Lempart *et al.,* 2019). Polyphosphates cause structural differences even in preformed fibrils which constitute changes in β-sheet packing within fibrils but not differences in strand-to-strand packing, and these nonetheless reduce the ability of polyphosphate-associated αS fibrils to associate with membranes and enter cells (Lempart *et al.,* 2019). Recent research by Yamaguchi *et al.* (2021) also shows that the secondary-structure changes induced by polyphosphates on αS fibrils are concentration-dependent, with thin versus thick fibrils predominating at low versus high polyphosphate concentrations, respectively. The concentration-dependency of the effect of polyphosphates on αS also extends to aggregation, as the aforementioned aggregate-enhancing effect actually occurs at multiple concentrations of ortho-, di-, tri-, tetra- and poly-phosphates (Yamaguchi *et al.,*

2021). Yamaguchi *et al.* (2021) show that these additives cause concentration-dependent increases in β-sheet-forming αS aggregation, measured as higher ThT fluorescence signals at plateau, which culminate in a maximum signal at lower polyphosphate concentrations. Beyond this maximum, the ThT fluorescence signals decrease, before rising again to a second maximum at higher polyphosphate concentrations (Yamaguchi *et al.,* 2021). These two distinct aggregation maxima likely result from electrostatic interactions at lower concentrations and Hofmeister salting-out effects at higher concentrations, the boundaries of which depend on the length of the polyphosphate chain (Yamaguchi *et al.,* 2021). Interestingly, the greater the number of phosphate groups, the more significant the aggregation maxima resulting from charge-charge interactions, suggesting that electrostatics and the overall concentration of negative charges are key drivers of αS aggregation in the presence of polyphosphates with more than two phosphate groups (Yamaguchi *et al.,* 2021). This conclusion is supported by the residue-specific interaction of αS and tetra-phosphates at concentrations less than 5 mM, which localizes to positively charged “KTK” segments, most specifically threonine residues, in the N-terminal αS KTKEGV repeats (Yamaguchi *et al.,* 2021). Yamaguchi *et al.* (2021) hypothesize, based on these results, that polyphosphate-driven charge-charge interactions disrupt long-range N- to C-terminal electrostatic contacts in αS monomers to cause compaction and fibril formation, although they do not provide experimental evidence to show phosphate-induced monomer conformational changes. However, research by Lempart *et al.* (2019) shows that the polyphosphate-fibril complexes are stable and resistant to phosphate hydrolysis, suggesting that polyphosphates may reduce αS cytotoxicity by attenuating fibril fragmentation and secondary nucleation. However,

the effect of polyphosphates on αS secondary nucleation is still unproven. Nonetheless, given the complex and potentially pathologically-relevant effect of polyphosphates on αS aggregation, the interactions and effects of biologically-relevant, phosphate-containing species like nucleotides on amyloid aggregation is an area of active research.

1.4 The Hydrotropic Effect of ATP on Liquid-Liquid Phase Separation and Protein Aggregation

Recent studies suggest that Adenosine Triphosphate (ATP), besides providing the majority of cellular energy through hydrolysis and serving as a source of phosphate in phosphorylation-dependent signalling, is also a modulator of liquid-liquid phase separation (LLPS) and protein solubility (Patel *et al.,* 2017; Sridharan *et al.,* 2019). Given that the classical functions of ATP require micromolar concentrations and yet cells maintain significantly higher overall ATP concentrations of 2-12 mM, it has been hypothesized that this energy-costly, millimolar excess of ATP is required for cells to control the condensation and aggregation of proteins (Dang *et al.,* 2021; Patel *et al.,* 2017). Indeed, yeast cells with artificially depleted ATP levels show pronounced aggregation of both intrinsic as well as extrinsic model proteins, highlighting the fact that normal ATP levels of approximately 4 mM are essential for maintaining protein solubility in living cells (Takaine *et al.,* 2022). Consequently, a substantial amount of recent research focuses on characterizing this novel function of ATP and determining the associate mechanism.

A popular, emerging hypothesis is that ATP is a biological hydrotrope, a small amphiphilic molecule that works at molar concentrations to increase the solubility of

hydrophobic molecules in solution, without aggregating itself (Patel *et al.,* 2017). This theory is supported by thermal proteome profiling studies of human immune cells, which show that ATP-Mg increases the solubility of approximately 25% of the insoluble proteome and preferentially targets positively-charged proteins that are enriched in disordered regions and have high isoelectric points (Sridharan *et al.,* 2019). Interestingly, this effect is not recapitulated by $MgCl_2$, suggesting that it is not predominantly salt driven and leading Sridharan *et al.* (2019) to hypothesize that ATP disrupts both π–π and electrostatic interactions in positively charged proteins to promote solubility via its aromatic adenine ring and its highly negatively charged phosphoanhydride bond. Consistent with this model, Patel *et al.* (2017) show that both the hydrophobic adenosine ring of ATP as well as its charged tripolyphosphate moiety are necessary for it to prevent the formation of and dissolve previously formed liquid droplets of fused-in-sarcoma (FUS), a protein related to neurodegenerative diseases including amyotrophic lateral sclerosis and frontotemporal dementia (Kang *et al.,* 2018). Moreover, this hydrotropic property of ATP is not recapitulated at equivalent concentrations of triphosphate or $MgCl_2$ (Patel *et al.,* 2017). This effect of ATP-Mg on LLPS is likely mechanistically similar to its ability to prevent the aggregation of amyloid-forming proteins such as synthetic Aß42 and the prion domain of Mot3. The latter is not recapitulated by NaCl and is not, therefore, likely to be predominantly salt-driven (Patel *et al.,* 2017). It is important to note that the processes of LLPS and amyloid aggregation are related for certain proteins like αS, for which LLPS nucleates aggregation (Ray *et al.,* 2020). Interestingly too, the solubilizing and fibril-dissolving effects of ATP on FUS are dissimilar to those of the known hydrotrope NaXS, providing a first indication that ATP, although it certainly has hydrotrope-like properties,

might be considered a “non-classical hydrotrope” (Patel *et al.,* 2017). In fact, ATP shows features atypical of classical hydrotropes. It fails standard solubility assays and it forms transient and highly dynamic dimers, trimers and oligomers at high concentrations (Mehringer *et al.,* 2021; Nishizawa *et al.,* 2021). Furthermore, while the hydrotropic function of ATP has been hypothesized to result from a general, non-specific interaction between ATP and proteins, there are exceptions (Nishizawa *et al.,* 2021). Unlike classical hydrotropes, ATP specifically binds a pocket of the FUS RNA-recognition motif with an average dissociation constant (K_d) of 3.77 ± 0.49 mM and thereby increases the kinetic barrier for fibrillization to inhibit FUS aggregation and LLPS (Kang *et al.,* 2018). This interaction involves the aromatic ring of adenine sitting in a hydrophobic pocket of FUS while the triphosphate moiety of ATP interacts electrostatically with a positively-charged protein pocket (Kang *et al.,* 2018). Thus, the solubility-enhancing effect of ATP appears to be widespread but nonetheless protein-specific, with specific ATP binding highly dependent on protein properties.

Whether or not ATP binds directly to a given protein has a profound impact on the mechanism by which it exerts its hydrotropic effect. Although ATP has no significant binding to the human eye-lens protein γS-crystallin, it is able to mediate the protein’s inter-molecular packing and thereby promote increased solubility in a manner that does not simply result from electrostatic screening, as NaCl does not show a similar effect (He *et al.,* 2020). The mechanism proposed to explain this effect involves ATP strongly interacting with water as well as dynamically interacting with the hydration shell of γS-crystallin molecules and thereby preventing their overlap or collapse (He *et al.,* 2020). Thus, ATP is able to antagonize the crowding-induced destabilization of γS-crystallin

without causing any significant conformational change (He *et al.,* 2020). By contrast, ATP as well as the ATP metabolite Adenosine Diphosphate (ADP) are able to prevent the aggregation of Amyloid-β Protein, inhibiting the formation of high-molecular-weight (HMW) oligomers, by direct binding and by inhibiting protein misfolding (Coskuner *et al.,* 2014; Pal and Paul, 2020). This reduced-misfolding effect of ATP on Amyloid-β is specific, is enhanced by the presence of equimolar Mg^{2+} and involves the adenosine group of ATP interacting with the aromatic region of Tyr_{10}, while the triphosphate moiety interacts with Ser_{26} in an energetically stable fashion (Coskuner *et al.,* 2014). ATP-Mg also interacts with the hydrophobic core region of Amyloid-β via hydrogen bonding, π−π stacking, and NH−π interactions that ultimately cause a dramatic decrease in the total β-sheet percentage of the protein (Pal and Paul, 2020). Likewise, ATP reduces the overall β-sheet content of human islet amyloid polypeptide (hIAPP) dimers and protofibrils from 18.43% to only 6.31%, while causing a corresponding increase solvent exposure as well as in coil percentage, which increases from 39 to 54% for dimers (Roy and Paul, 2021). This change in secondary structure for hIAPP is aggregation-inhibiting and, as for Amyloid-β, involves both the adenosine and triphosphate groups of ATP interacting with the protein, although for hIAPP this interaction is primarily driven by the hydrophobic ring and the amino group in the adenine and the hydroxyl group in the ribose (Roy and Paul, 2021). Therefore, an emerging pattern to explain the specific interaction between ATP and proteins involves the aromatic nitrogenous base of ATP selectively interacting with uncharged protein residues via hydrophobic interactions, while the negatively charged phosphate groups interact predominantly with polar and positively-charged residues (Sarkar and Mondal, 2021). As such, ATP preferentially stabilizes polymers with regions

of overall positive and negative charge that also contain hydrophobic patches, thereby inhibiting their aggregation (Sarkar and Mondal, 2021).

1.5 The Aggregation- and LLPS-Promoting Effect of ATP on Specific Proteins

Despite its hydrotrope-like properties, ATP can also decrease protein solubility and enhance aggregation, depending on the protein in question (Sridharan *et al.,* 2019). For instance, adenine polyphosphates increase the aggregation rate of partially unfolded human muscle acylphosphatase (AcP) in a manner that depends on the length and overall charge of the polyanion, as increasing the number of phosphate groups from one (adenosine monophosphate, AMP) to two (ADP) or three (ATP) causes a sequential reduction in the lag time of AcP aggregation (Calamai *et al.,* 2006). This effect is also modulated by Mg^{2+}, as 100 mM $MgSO_4$ causes a dramatic reduction in anion-induced Thioflavin T (ThT) fluorescence, and likewise inhibits the high affinity binding between ATP and preformed AcP fibrils (Calamai *et al.,* 2006). Coupled with the fact that the AcP-ATP interaction is suppressed in the presence of increased ionic strength, these results suggest that electrostatics drive binding (Calamai *et al.,* 2006). Similarly, ATP exerts an electrostatically-driven, pro-aggregation effect on the amyloid protein Tau, which, like AcP, has a net positive charge at physiological pH 7.4 (Calamai *et al.,* 2006; Heo *et al.,* 2020). Since 0.1 – 10 mM ATP and triphosphate exhibit a similar concentration-dependent, pro-aggregation effect on Tau that is not mirrored by adenosine, this effect is thought to proceed via the phosphate groups of ATP attracting and non-specifically bridging lysine residues of multiple Tau monomers to bring them together and cause dimerization that accelerates fibril elongation by forming reactive nuclei (Heo *et al.,* 2020).

In addition, the lysine charge neutralization by ATP enhances Tau self-assembly likely by reducing charge-charge repulsion between Tau monomers and thereby increasing the probability of aggregate nucleation and fibril elongation (Heo *et al.,* 2020). Moreover, the dimerization and subsequent full-scale aggregation of Tau also occurs in SHSY5Y and HEK293 cells with elevated ATP levels, thus highlighting the biological- and pathological relevance of this effect (Heo *et al.,* 2020). Across the proteome, ATP also decreases the solubility of select proteins, including the PD-related protein NUCKS1, and enhances the phase separation of the autism-related protein CAPRIN1 at concentrations above 0.25 mM (Kim *et al.,* 2021; Sridharan *et al.,* 2019). It is reasonable to assume, therefore, that the effect of ATP is related to these disorders, particularly PD, as physiological concentrations of ATP-Mg up to 10 mM also enhance the oligomerization of PD-related protein TDP-43 (Wang *et al.,* 2019). Interestingly, this effect is due to the specific binding of ATP to the TDP-43 N-terminal domain, an interaction that is also likely electrostatic as it is modulated by NaCl, and is therefore similar to the specific binding of ATP to the arginine-rich regions of CAPRIN1 (Kim *et al.,* 2021; Wang *et al.,* 2019). Thus, the pro-aggregation effect of ATP is similar to its hydrotropic effect in that it depends on specific protein properties and binding. However, the importance of the triphosphate moiety and electrostatics appears more significant to ATP-mediated aggregation-enhancement than inhibition.

1.6 The Bi-Phasic Effect of ATP on the LLPS of Specific Disease-Related Proteins

Interestingly, the hydrotrope-like effect of ATP on a particular protein is not mutually exclusive to its ability to decrease protein solubility (Dang *et al.,* 2021). Recent

studies suggest that ATP can both enhance and inhibit the LLPS of FUS in a manner that critically depends on whether the ATP concentration is below or above a physiologically-relevant threshold (Kang *et al.,* 2018). In the case of FUS, the threshold beyond which the effect of ATP-Mg changes is approximately 2 mM. At concentrations less than 2 mM, ATP-Mg increases both the number and maximal diameter of FUS LLPS droplets by almost four-fold, while at concentrations between 2 – 10 mM, ATP-Mg decreases both the number and size of the droplets until, by 8 mM, they are completely dissolved (Kang *et al.,* 2018). Importantly, this dual effect of ATP-Mg requires both the N-terminal domain of FUS, which contains a QGSY-rich prion-like domain as well as an RG/RGG-rich region, and the RG/RGG-rich C-terminal domain, as the N-terminal domain alone shows only a decrease in LLPS by ATP-Mg, regardless of concentration (Kang *et al.,* 2018). The proposed mechanism to explain this duality involves the bivalent binding of ATP-Mg to FUS at lower concentrations to form large and dynamic complexes that manifest as LLPS droplets, while at higher ATP-Mg concentrations the saturation of FUS with ATP-Mg disrupts the dynamic complexes, causing their dissolution (Kang *et al.,* 2018). Therefore, the effect of ATP-Mg likely stems from the direct, bivalent binding of ATP-Mg to FUS, binding which is hypothesized to involve the adenine ring forming π-π interactions with aromatic protein sidechains, while the triphosphate moeity interacts electrostatically with the side chains of arginine and lysine residues (Kang *et al.,* 2018). In this respect, the biphasic effect of ATP-Mg on FUS LLPS is similar to the concentration-dependent effect of polyphosphates on αS aggregation, suggesting that the electrostatic interaction between ATP-Mg and FUS might also be driven by different factors, e.g., charge-charge interactions versus salting-out effects, at low versus high concentrations (Kang *et al.,*

2018; Yamaguchi *et al.,* 2021). However, the mechanisms underlying the different concentration-dependent effects of ATP on proteins are still unclear.

1.7 The Connection Between ATP and αS

A growing body of evidence suggests that, given its effect on the aggregation and LLPS of multiple proteins related to neurogenerative disease, ATP likely plays a critical role in the pathophysiology of αS (Takaine *et al.,* 2022; Wang *et al.,* 2007). However, the molecular mechanisms accounting for this complex role remain unclear. Some studies report that an artificial increase in ATP levels from 4 to 5.5 mM reduces the aggregation and toxicity of αS in multiple yeast strains, suggesting that high ATP levels promote increased αS solubility (Takaine *et al.,* 2022). By contrast, Wang *et al.* (2007) report that elevated ATP levels lead to significant accumulation or aggregation of αS in transgenic *C. elegans*. Under *in vitro* conditions, however, ATP concentrations less than 2 mM do not significantly affect the fibrillization kinetics of WT αS as measured by the amyloid-specific dye ThT (Heo *et al.,* 2020). It is likely, therefore, that the effect of ATP on αS β-sheet fibril formation is similar to its effect on the LLPS of FUS in that it is concentration-dependent, involving a threshold beyond which the effect of ATP potentially changes from aggregation-inhibiting to enhancing or *vice versa*. However, thorough studies on the concentration-dependent effect of ATP on αS aggregation are still lacking. Specifically, it is not yet known whether physiologically-relevant ATP concentrations of 0 – 12 mM exert different effects on early- versus late-stage αS aggregation, what drives these effects, whether they are modulated by Mg^{2+} and whether they affect fibril morphology. In addition,

it is unclear whether ATP affects the αS aggregation pathway, *e.g*., whether it specifically targets monomers, oligomers or fibrils, and/or processes such as secondary nucleation.

One study by Nishizawa *et al.* (2021) established that ATP binds differently to WT αS monomers at low versus high concentrations, displaying a sigmoidal binding isotherm with an inflection point at approximately 3 mM, thereby supporting the hypothesis of a threshold-dependent effect of ATP on αS. These authors also determine that the nucleobase of ATP is likely not the key driver of the ATP-αS interaction, as ATP, GTP, CTP and UTP show similar Nuclear Magnetic Resonance (NMR)-based αS chemical shifts (Nishizawa *et al.,* 2021). These observations suggest that the phosphate groups are relevant to the ATP-αS interaction, as confirmed by the NMR-based αS chemical shifts induced by ATP, which are significantly different from those induced by adenosine and ribose-5-phosphate (Nishizawa *et al.,* 2021). Finally, these authors show that the addition of ATP to αS monomers in the presence of 10 mM $MgCl_2$ causes shifts in primarily the C-terminus, leading them to hypothesize that Mg^{2+} binding to the C-terminal metal ion binding site in αS bridges the interaction between ATP and αS (Nishizawa *et al.,* 2021). Overall, they conclude that ATP binds to WT αS monomers via weak, general, non-specific, non-covalent interactions (Nishizawa *et al.,* 2021). However, these interactions are not fully characterized (Nishizawa *et al.,* 2021). Furthermore, it is not yet known whether the αS-ATP interaction is modulated by physiologically-relevant conditions like salt and Mg^{2+}, and whether or not ATP binding modulates the overall conformation of αS monomers by disrupting long-range electrostatic N- to C-terminal contacts, as was hypothesized for polyphosphates (Yamaguchi *et al.,* 2021).

1.8 Thesis Outline

1.8.1 Thesis Goal

ATP has been shown to either increase or decrease the solubility of WT αS, depending on the experimental conditions (Takaine *et al.,* 2022; Wang *et al.,* 2007). However, the exact mechanism by which ATP modulates the solubility of αS is currently not fully understood and a detailed study of the concentration-dependent effect of ATP on pathologically-relevant αS aggregation is still lacking. Based upon published models describing the interaction of ATP with proteins, it is possible to hypothesize that the aromatic purine ring of ATP clusters over hydrophobic patches in the NAC region of αS, while the triphosphate chain interacts with bulk water to prevent the formation of full-scale aggregates by electrostatically repelling other such bound monomers (Figure 1b) (Song, 2021). By contrast, the pro-aggregation effect of ATP on αS could arise via the phosphate-driven bridging of multiple αS monomers to nucleate fibril formation, as is the case for Tau (Figure 1c) (Heo *et al.,* 2020). Elucidating which of these models best describes the interaction between ATP and αS is fundamentally important for determining whether the overall effect of ATP is to enhance or inhibit pathologically-relevant αS aggregation. Knowing this could potentially also explain why advancing age is the greatest risk factor for idiopathic PD development, as ATP levels decline dramatically with age in many model species and are decreased in the brains of patients with early PD (Chaudhari and Kipreos, 2018; Reeve *et al.,* 2014; Takaine *et al.,* 2022). Since the interactions between ATP and proteins are dynamic and highly residue-specific, this makes NMR spectroscopy an ideal tool to probe such interactions, especially since αS is intrinsically disordered (Bisi *et al.,* 2021).

Therefore, the aim of this study is to explore, at a residue-specific level, how ATP modulates the solubility of WT αS (Chapter 3) as well as the PD-related variants E46K and A53T (Chapter 4) and whether it exerts a different effect on αS monomers versus aggregates. Addressing this gap is critical to understanding the multiple physiological roles of ATP and for exploiting the solubility-modulating properties of ATP for biopharmaceutical formulations. In addition, we aim to characterize the role of the ATP phosphates and the Mg^{2+} counterion on ATP-αS binding and to understand if direct binding interactions of ATP-Mg with αS modulate long-range αS interactions. Finally, our goal is to perform a concentration-dependent analysis of how ATP affects both early- and late-stage αS β-sheet fibril formation, since these events are critical for PD development (Hoyer *et al.,* 2002).

To accomplish these experimental goals, we will rely on NMR spectroscopy to characterize the interactions between ATP, AMP, ADP, triphosphate and αS both in the absence and presence of $MgCl_2$. Specifically, we will use ^{1}H-^{15}N Heteronuclear Single Quantum Coherence Spectroscopy or HSQC experiments to map the αS residue-specific shifts and intensity changes caused by these additives. In addition, we will use intramolecular Paramagnetic Relaxation Enhancement or PRE experiments and 1D Saturation Transfer Difference (STD) experiments to probe how ATP and other additives affect long-range electrostatic contacts in αS monomers and how they interact with WT αS oligomers, respectively. To characterize the effect of ATP on αS aggregate formation, we will employ Dynamic Light Scattering (DLS), ThT fluorescence and Negative Stain Transmission Electron Microscopy (TEM). Lastly, we will use NMR-based transverse ^{15}N amide relaxation R_2 experiments to characterize the αS monomer-fibril interactions

underlying secondary nucleation in the presence of ATP. Overall, we hope that this study will clarify key outstanding questions regarding the interaction of ATP and αS, while providing insight into a possible age-related factor in PD development and pathology, *i.e.,* ATP levels.

1.8.2 Chapter Outlines

Chapter 2 focuses on the NMR spectroscopy, fluorescence, light scattering, microscopy and electrophoretic experimental methodology used to investigate the interaction mechanism between ATP and αS as well as the effect of ATP on αS aggregation. This chapter discusses in detail protein expression and purification, the preparation of αS oligomers and fibrils, NMR sample preparation as well as the experimental setup and parameters for NMR experiments including HSQCs, STDs, PREs and R_2. Additionally, this chapter details two analysis methods for NMR experimental data – CHESPA and pairwise chemical shift projection analysis – as well as the setup of ThT fluorescence, DLS, SEC-MALS and SDS-PAGE experiments.

Chapters 3 and 4 describe and discuss the experimental results of the study. Chapter 3 focuses on the results pertaining to WT αS, while chapter 4 describes those involving the PD-related αS variants E46K and A53T. The results are mainly grouped into sections according to each of the figures. First, NMR-based chemical shifts establish that the triphosphate moiety of ATP drives its electrostatic interaction with the N-terminal Thr-rich pseudo-apolipoprotein-like repeats of αS monomers. This interaction, moreover, is modulated by Mg^{2+}, according to the residue-specific shifts and CHESPA analysis. PREs, residue-specific NMR intensity losses and time-dependent ThT fluorescence experiments

reveal that ATP disrupts long-range N- to C-terminal electrostatic contacts in αS monomers in a phosphate-dependent manner to enhance initial aggregation, while plateau ThT experiments and TEM suggest that ATP inhibits late-stage αS cross-β-sheet fibril formation in a manner that requires two or more phosphate groups. R_2 experiments indicate that ATP inhibits N-terminally-driven αS monomer-fibril interactions. These results are collectively analyzed and used to construct a proposed model to explain how the ATP-αS interaction influences αS aggregation. Finally, similar experiments as above but involving E46K and A53T αS instead of WT establish that the effect of ATP on these PD-related variants is remarkably different than its effect on WT, particularly in terms of aggregation. Given the connection between ATP and PD, the relevance of ATP to E46K and A53T αS PD-related pathology is discussed based on these results.

Lastly, chapter 5 outlines the conclusions and future directions for analyzing the effect of ATP on αS. Given the cytotoxicity of αS oligomers, the biological relevance of αS-lipid interactions as well as the pathological relevance of αS LLPS, foundational experiments designed to elucidate the effect of ATP on αS oligomer structure and toxicity, the possible modulation of αS-membrane binding by ATP and its effect on αS aggregation-nucleating LLPS are discussed.

1.9 References

Ahmed, R., Huang, J., Weber, D.K., Gopinath, T., Veglia, G., Akimoto, M., Khondker, A., Rheinstädter, M.C., Huynh, V., Wylie, R.G., Bozelli Jr., J.C., Epand, R.M., and Melacini, G. (2020) Molecular mechanism for the suppression of alpha synuclein membrane toxicity by an unconventional extracellular chaperone. *J. Am. Chem. Soc. 142,* 9686-9699.

Ahmed, R., VanSchouwen, B., Jafari, N., Ni, X., Ortega, J., and Melacini, G. (2017) Molecular mechanism for the (−)-epigallocatechin gallate-induced toxic to nontoxic remodeling of aβ oligomers. *J. Am. Chem. Soc. 139,* 13720-13734.

Alam, M.M., Yang, D., Li, X-Q., Liu, J., Back, M.C., Trivett, A., Karim, B., Barbut, D., Zasloff, M., and Oppenheim, J.J. (2022) Alpha synuclein, the culprit in Parkinson disease, is required for normal immune function. *Cell. Rep. 38,* 110090.

Alza, N.P., González, P.A.I., Conde, M.A., Uranga, R.M., and Salvador, G.A. (2019) Lipids at the crossroad of α-synuclein function and dysfunction: biological and pathological implications. *Front. Cell. Neurosci. 13,* doi: 10.3389/fncel.2019.00175.

Bisi, N., Feni, L., Peqini, K., Pérez-Peña, H., Ongeri, S., Pieraccini, S., and Pellegrino, S. (2021) α-synuclein: an all-inclusive trip around its structure, influencing factors and applied techniques. *Front. Chem. 9,* 666585.

Boyer, D.R., Li, B., Sun, C., Fan, W., Zhou, K., Hughes, M.P., Sawaya, M.R., Jiang, L., and Eisenberg, D.S. (2020) The α-synuclein hereditary mutation E46K unlocks a more stable, pathogenic fibril structure. *PNAS. 117,* 3592-3602.

Bozelli Jr., J.C., Kamski-Hennekam, E., Melacini, G., and Epand, R.M. (2021) α-Synuclein and neuronal membranes: conformational flexibilities in health and disease. *Chem. Phys. Lipids. 235,* 105034.

Buell, A.K., Galvagnion, C., Gaspar, R., Sparr, E., Vendruscolo, M., Knowles, T.P.J., Linse, S., and Dobson, C.M. (2014) Solution conditions determine the relative importance of nucleation and growth processes in α-synuclein aggregation. *PNAS. 111,* 7671-7676.

Calamai, M., Kumita, J.R., Mifsud, J., Parrini, C., Ramazzotti, M., Ramponi, G., Taddei, N., Chiti, F., and Dobson, C.M. (2006) Nature and significance of the interactions between amyloid fibrils and biological polyelectrolytes. *Biochemistry-US. 45,* 12806-12815.

Chaudhari, S.N., and Kipreos, E.T. (2018) The energy maintenance theory of aging: maintaining energy metabolism to allow longevity. *Bioessays. 40,* e1800005.

Chen, S.W., Drakulic, S., Deas, E., Ouberai, M., Aprile, F.A., Arranz, R., Ness, S., Roodveldt, C., Guilliams, T., De-Genst, E.J., Klenerman, D., Wood, N.W., Knowles, T.P.J., Alfonso, C., Rivas, G., Abramov, A.Y., Valpuesta, J.M., Dobson, C.M., and Cremades, N. (2015) Structural characterization of toxic oligomers that are kinetically trapped during α-synuclein fibril formation. *PNAS. 112,* E1994-E2003.

Cho, M-K., Kim, H-Y., Fernandez, C.O., Becker, S., and Zweckstetter, M. (2011) Conserved core of amyloid fibrils of wild type and A30P mutant α-synuclein. *Protein. Sci. 20,* 387-395.

Cohlberg, J.A., Li, J., Uversky, V.N., and Fink, A.L. (2002) Heparin and other glycosaminoglycans stimulate the formation of amyloid fibrils from alpha-synuclein *in vitro. Biochemistry. 41,* 1502-1511.

Coskuner, O., and Murray, I.V.J. (2014) Adenosine triphosphate (ATP) reduces amyloid-β protein misfolding *in vitro*. *J. Alzheimers. Dis. 41,* 561-574.

Dang, M., Lim, L., Kang, J., and Song, J. (2021) ATP biphasically modulates LLPS of TDP-43 PLD by specifically binding arginine residues. *Communications. Biology. 4,* 714.

Daturpalli, S., Waudby, C.A., Meehan, S., and Jackson, S.E. (2013) Hsp90 inhibits α-synuclein aggregation by interacting with soluble oligomers. *J. Mol. Biol. 425,* 4614-4628.

de Oliveira, G.A.P., and Silva, J.L. (2019) Alpha-synuclein stepwise aggregation reveals features of an early onset mutation in parkinson's disease. *Commun. Biol. 2,* 374.

Dettmer, U., Newman, A.J., von Saucken, V.E., Bartels, T., and Selkoe, D. (2015) KTKEGV repeat motifs are key mediators of normal α-synuclein tetramerization: their mutation causes excess monomers and neurotoxicity. *PNAS. 112,* 9596-9601.

Furukawa, K., Aguirre, C., So, M., Sasahara, K., Miyanoiri, Y., Sakurai, K., Yamaguchi, K., Ikenaka, K., Mochizuki, H., Kardos, J., Kawata, Y., and Goto, Y. (2020) Isoelectric

point-amyloid formation of α-synuclein extends the generality of the solubility and supersaturation-limited mechanism. *CRSB. 2,* 35-44.

Fusco, G., Chen, S.W., Williamson, P.T.F., Cascella, R., Perni, M., Jarvis, J.A., Cecchi, C., Vendruscolo, M., Chiti, F., Cremades, N., Ying, L., Dobson, C.M., and De Simone, A. (2017) Structural basis of membrane disruption and cellular toxicity by α-synuclein oligomers. *Science. 358,* 1440-1443.

Golts, N., Snyder, H., Frasier, M., Theisler, C., Choi, P., and Wolozin, B. (2002) Magnesium inhibits spontaneous and iron-induced aggregation of α-synuclein. *J. Biol. Chem. 277,* 16116-16123.

He, Y., Kang, J., and Song, J. (2020) ATP antagonizes the crowding-induced destabilization of the human eye-lens protein γS-crystallin. *Biochem. Biophys. Res. Commun. 526,* 1112-1117.

Heo, C.E., Han, J.Y., Lim, S., Lee, S., Im, D., Lee, M.J., Kim, Y.K., and Kim, H.I. (2020) ATP kinetically modulates pathogenic tau fibrillizations. *ACS. Chem. Neurosci. 11,* 3144-3152.

Holec, S.A.M., Liu, S.L., and Woerman, A.L. (2022) Consequences of variability in α-synuclein fibril structure on strain biology. *Acta. Neuropathol. 143,* 311-330.

Hoyer, W., Antony, T., Cherny, D., Heim, G., Jovin, T.M., and Subramaniam, V. (2002) Dependence of a-synuclein aggregate morphology on solution conditions. *J. Mol. Biol. 322,* 383-393.

Hoyer, W., Cherny, D., Subramaniam, V., and Jovin, T.M. (2004) Impact of the acidic c-terminal region comprising amino acids 109-140 on α-synuclein aggregation *in vitro*. *Biochemistry. 43,* 16233-16242.

Kang, J., Lim, L., and Song, J. (2018) ATP enhances at low concentrations but dissolves at high concentrations liquid-liquid phase separation (LLPS) of ALS/FTD-causing FUS. *Biochem. Bioph. Res. Co. 504,* 545-551.

Kim, T.H., Payliss, B.J., Nosella, M.L., Lee, I.T.W., Toyama, Y., Forman-Kay, J.D., and Kay, L.E. (2021) Interaction hot spots for phase separation revealed by NMR studies of a CAPRIN1 condensed phase. *PNAS. 118,* e2104897118.

Kumari, P., Ghosh, D., Vanas, A., Fleischmann, Y., Wiegand, T., Jeschke, G., Riek, R., and Eichmann, C. (2021) Structural insights into α-synuclein monomer–fibril interactions. *PNAS. 118,* e2012171118.

Lempart, J., Tse, E., Lauer, J.A., Ivanova, M.I., Sutter, A., Yoo, N., Huettemann, P., Southworth, D., and Jakob, U. (2019) Mechanistic insights into the protective roles of polyphosphate against amyloid cytotoxicity. *Life. Sci. Alliance. 2,* e201900486.

Mehringer, J., Do, T-M., Touraud, D., Hohenschutz, M., Khoshsima, A., Horinek, D., and Kunz, W. (2021) Hofmeister verses neuberg: is ATP really a biological hydrotrope? *Cell. Reports. 2,* 100343.

Moons, R., Konijnenberg, A., Mensch, C., Van Elzen, R., Johannessen, C., Maudsley, S., Lambeir, A-M., and Sobott, F. (2020) Metal ions shape α-synuclein. *Sci. Rep. 10,* 16293.

Nishizawa, M., Walinda, E., Morimoto, D., Kohn, B., Scheler, U., Shirakawa, M., and Sugase, K. (2021) Effects of weak nonspecific interactions with ATP on proteins. *J. Am. Chem. Soc. 143,* 11982-11993.

Pal, S., and Paul, S. (2020) ATP controls the aggregation of $A\beta_{16-22}$ Peptides. *J. Phys. Chem. B. 124,* 210-223.

Patel, A., Malinovska, L., Saha, S., Wang, J., Alberti, S., Krishnan, Y., and Hyman, A.A. (2017) ATP as a biological hydrotrope. *Science. 356,* 753-756.

Prahl, J., Pierce, S.E., Coetzee, G.A., and Tyson, T. (2022) Alpha-synuclein negatively controls cell proliferation in dopaminergic neurons. *Mol. Cell. Neurosci. 119,* 103702.

Ramis, R., Ortega-Castro, J., Vilanova, B., Adrover, M., and Frau, J. (2020) Unraveling the NaCl concentration effect on the first stages of α-synuclein aggregation. *Biomacromolecules. 21,* 5200-5212.

Ray, S., Singh, N., Kumar, R., Patel, K., Pandey, S., Datta, D., Mahato, J., Panigrahi, R., Navalkar, A., Mehra, S., Gadhe, L., Chatterjee, D., Sawner, A.S., Maiti, S., Bhatia, S., Gerez, J.A., Chowdhury, A., Kumar, A., Padinhateeri, R., Riek, R., Krishnamoorthy, G., and Maji, S.K. (2020) α-Synuclein aggregation nucleates through liquid–liquid phase separation. *Nat. Chem. 12,* 705-716.

Reeve, A., Simcox, E., and Turnbull, D. (2014) Ageing and parkinson's disease: why is advancing age the biggest risk factor? *Ageing. Res. Rev. 14,* 19-30.

Rietdijk, C.D., Perez-Pardo, P., Garssen, J., van Wezel, R.J.A., and Kraneveld, A.D. (2017) Exploring braak's hypothesis of parkinson's disease. *Front. Neurol. 8,* 37.

Roy, R., and Paul, S. (2021) Potential of ATP toward prevention of hIAPP oligomerization and destabilization of hIAPP protofibrils: an *in silico* perspective. *J. Phys. Chem. 125,* 3510-3526.

Sarkar, S., and Mondal, J. (2021) Mechanistic insights on ATP's role as a hydrotrope. *J. Phys. Chem. 125,* 7717-7731.

Sawada, M., Yamaguchi, K., Hirano, M., Noji, M., So, M., Otzen, D., Kawata, Y., and Goto, Y. (2020) Amyloid formation of α-synuclein based on the solubility- and supersaturation-dependent mechanism. *Langmuir. 36,* 4671-4681.

Song, J. (2021) Adenosine triphosphate energy-independently controls protein homeostasis with unique structure and diverse mechanisms. *Protein. Sci. 30,* 1277-1293.

Sridharan, S., Kurzawa, N., Werner, T., Gunthner, I., Helm, D., Huber, W., Bantscheff, M., and Savitski, M.M. (2019) Proteome-wide solubility and thermal stability profiling reveals distinct regulatory roles for ATP. *Nat. Commun. 10,* 1155.

Stephens, A.D., Zacharopoulou, M., Moons, R., Fusco, G., Seetaloo, N., Chiki, A., Woodhams, P., Mela, I., Lashuel, H.A., Phillips, J.J., De Simone, A., Sobott, F., and Kaminski Schierle, G.S. (2020) Extent of N-terminus exposure of monomeric alpha-synuclein determines its aggregation propensity. *Nat. Commun. 11,* 1-15.

Takaine, M., Imamura, H., and Yoshida, S. (2022) High and stable ATP levels prevent aberrant intracellular protein aggregation in yeast. *eLife. 11,* e67659.

Wang, L., Lim, L., Dang, M., and Song, J. (2019) A novel mechanism for ATP to enhance the functional oligomerization of TDP-43 by specific binding. *Biochem. Biophys. Res. Commun. 514,* 809-814.

Wang, Y-M., Pu, P., and Le, W-D. (2007) ATP depletion is the major cause of MPP+ induced dopamine neuronal death and worm lethality in alpha-synuclein transgenic *C. elegans. Neurosci. Bull. 6,* 329-335.

Yamaguchi, K., So, M., Aguirre, C., Ikenaka, K., Mochizuki, H., Kawata, Y., and Goto, Y. (2021) Polyphosphates induce amyloid fibril formation of α-synuclein in concentration-dependent distinct manners. *J. Biol. Chem. 296,* 100510.

Chapter 2

Materials and Methods

2.1 Recombinant Alpha-Synuclein Expression and Purification

Expression and purification of recombinant WT, S87C, A53T, E46K and E46K S87C alpha-synuclein protein was accomplished by following a published protocol (Hoyer *et al.,* 2002) with slight modifications. Briefly, *E. coli* BL21(DE3) cells transformed with the pT7-7 plasmid harboring either the WT or the S87C point mutation-containing the Alpha-synuclein sequence were grown at 37 ºC with shaking either in Luria–Bertani medium (for preparation of unlabelled protein for ThT and fibril experiments) or isotope-enriched M9 minimal media containing 1 g/L of ^{15}N-ammonium chloride (for preparation of ^{15}N-labelled protein) and, in both cases, 100 µg/mL of ampicillin. After reaching an OD_{600} of ~0.6-0.8, αS expression was induced with 100 µM isopropyl β-D-1-thiogalactopyranoside (IPTG) at 37 °C with shaking for 4-5 hrs and cells were pelleted by centrifugation at 3836 X g. Cell pellets were stored at -80ºC until use. After resuspending cell pellets in lysis buffer (10 mM Tris-HCl, 1 mM EDTA, 1 mM AEBSF protease inhibitor 101500 from EMD Millipore, pH 8), cells were lysed via three freeze-thaw cycles followed by sonication and heating to >100°C for 20 min. Cell lysates were centrifuged at 12326 X g for 1 hr to pellet cell debris, at which point 10 mg/mL streptomycin sulfate was added to the supernatant, which was then stirred for 20 min at 4 °C followed by further centrifugation at 20376 X g for 20 min to pellet nucleic acids. Alpha-synuclein protein was precipitated from the supernatant by adding 360 mg/mL ammonium sulfate and stirring for 20 min at 4 °C. After centrifuging the mixture at 20376 X g for 20 min, the resulting pellet was resuspended in

25 mM Tris-HCl, pH 7.7, placed in 3.5 kDa-cutoff dialysis tubing and dialyzed against 5 L of the same buffer for 2 hr to remove any remaining ammonium sulfate. The dialyzed protein was then filtered with a 0.2 µM filter and loaded onto an anion exchange column (HiTrap Q Sepharose high performance, GE Healthcare) and eluted with a 0−600 mM NaCl step gradient. Purified αS eluted at ~300 mM NaCl and was concentrated using a 10 kDa Amicon centrifugal filter unit, filtered as before and then loaded onto a Hiload 16/600 Superdex 200 column pre-equilibrated with either milliQ H_2O, NMR buffer (50 mM Hepes, 5% D_2O, pH 7.4), ThT buffer (20 mM K_2HPO_4, 5 mM KH_2PO_4, 100 mM KCl, 200 µM EDTA, 0.05% NaN_3, pH 7.4) or fibril buffer (1X PBS, 0.05% NaN_3, pH 7.4) (Ahmed *et al.,* 2020; Wördehoff and Hoyer, 2018). The eluted protein was then concentrated using another 10 kDa Amicon centrifugal filter unit. The final protein concentration was confirmed by A_{280} measurements using an extinction coefficient of 5600 M^{-1} cm^{-1} (Fusco *et al.,* 2017).

2.2 Preparation of WT αS oligomers

To form kinetically trapped αS oligomers, lyophilized, monomeric αS prepared in milliQ H_2O was dissolved in 1X PBS, 100% D_2O, pH 7.4, filtered using a 0.2 µM filter to remove any insoluble species and incubated at 800 µM in a sealed container at 37 ºC for 20-24 hrs, as described previously (Chen *et al.,* 2015). The resulting aggregate mixture was extensively filtered using a 50 kDa Amicon centrifugal filter unit to remove monomers and the final protein concentration of the supernatant was estimated by A_{280} measurements using the extinction coefficient for αS monomers of 5600 M^{-1} cm^{-1} (Fusco *et al.,* 2017). The protein concentration was adjusted to 68.57 µM using the above PBS

buffer and placed in a 3 mm NMR tube for analysis. Subsequent 1D STD/STR experiments in the presence of increasing concentrations of ATP were performed after the addition of ATP to the above oligomer sample.

2.3 Preparation of WT αS fibrils

Formation of late-stage αS fibrils was accomplished by incubating 1.5 mL Eppendorf tubes containing 500 µL aliquots of 500 µM monomeric αS protein prepared in fibril buffer at 37 ºC in a rotating incubator at approximately 200 rpm for 2-3 weeks, following the general protocol of Kumari *et al.* 2021. Fibrils were then pelleted by ultracentrifugation at 121968 X g for 1 hr at 4 ºC, the supernatant was removed, and the ultracentrifugation was repeated after resuspending the fibrils in 1.2 mL of NMR buffer. Pellets were stored at 4 ºC for not more than two weeks until use, whereupon the fibril pellet was washed two times with NMR buffer to remove salt and resuspended until homogenous in NMR buffer. The fibril concentration was approximated using the equivalent monomer concentration, calculated based on A_{280} measurements using an extinction coefficient of 5600 M^{-1} cm^{-1} (Fusco *et al.,* 2017).

2.4 Solution NMR Spectroscopy

All solution NMR spectra were recorded using a Bruker AV 700 spectrometer equipped with a TCI cryo-probe at approximately 10ºC and were analyzed with TopSpin 4.0.9., and Sparky using Gaussian line-fitting. Additional details are discussed below.

2.4.1 ^{1}H-^{15}N Heteronuclear Single Quantum Coherence (HSQCs)

The residue-specific effects of ATP and ATP analogs on αS monomers were monitored by two-dimensional ^{1}H-^{15}N HSQC NMR experiments with water suppression using a 3-9-19 pulse sequence with gradients, recorded with a recycling delay d_1 of 1s, 8 scans, and 4K (t_2) and 300 (t_1) complex points for spectral widths of 16.2 ppm (^{1}H) and 35.0 ppm (^{15}N), respectively. Spectra were acquired at 283K, while chemical shifts and intensity changes were measured through Gaussian fitting of the peaks in Sparky. Stock solutions of AMP, ADP, ATP, Sodium Triphosphate (purchased from Sigma-Aldrich) and salts $MgCl_2$ and NaCl (purchased from Alfa Aesar and Fisher Scientific) were prepared on ice in NMR buffer with pH adjusted to 7.4 using NaOH and HCl. ATP-Mg was prepared on ice by dissolving equimolar amounts of ATP and $MgCl_2$ into NMR buffer and incubating overnight on a rocker at 4 ºC before adjusting the pH to 7.4 as above. Samples of fresh, 120 µM ^{15}N WT αS monomers in NMR buffer were prepared in 5 mm NMR tubes in the presence or absence of increasing concentrations of ATP, ATP-Mg, $MgCl_2$ or ATP analogs and in 3 mm NMR tubes in the absence or presence of 150 mM NaCl. For experiments with Mg- or ATP-bound αS, samples of αS in NMR buffer with either 10 mM $MgCl_2$ or ATP were incubated overnight on a rocker at 4 ºC before the addition of the other additive. Compounded chemical shifts were calculated using the formula $\Delta CCS = (0.5*((\delta H_{Additive} - \delta H_{No\ Additive})\text{^}2 + (0.15*(\delta N_{Additive} - \delta N_{No\ Additive})\text{^}2)))\text{^}1/2$. Deviations from this formula are outlined in specific figure captions. In specific cases, the chemical shift data were fitted to the one-site specific binding model in GraphPad Prism 8.4.2., with the model-calculated approximate K_ds shown and errors either estimated as per the similar

work of Selvaratnam *et al.* (2011) or represented by the standard deviations of all residues in a given sample (for Figure 2g).

2.4.2 CHEmical Shift Projection Analysis (CHESPA)

The CHESPA analysis involved ^{1}H-^{15}N HSQCs acquired as described above for three samples: fresh 120 µM ^{15}N WT αS in NMR buffer in the absence or presence of 10 mM ATP or ATP-Mg. The reference CHESPA vector was defined as that from the αS sample to the sample of αS with 10 mM ATP, and the perturbation CHESPA vector was defined as that from the sample of αS with 10 mM ATP to the sample of αS and 10 mM ATP-Mg. The angle between the perturbation and the reference vector is denoted as θ, and is defined as per equation 6 in Boulton *et al.* 2014. The CHESPA analysis was performed in Sparky using a scaling factor of 0.15 for the ^{15}N dimension and a cut-off of 0.001 ppm. A detailed description of the CHESPA analysis is reported by Shao *et al.* (2021).

2.4.3 Intramolecular Paramagnetic Relaxation Enhancement (PRE) to Probe αS Monomer Unfolding in the Presence of ATP and ATP Analogs

The effect of ATP and ATP analogs on long-range electrostatic contacts between the N- and C-termini of αS monomers was probed using 120 µM samples of monomeric ^{15}N S87C αS spin-labeled with non-acetylated MTSL (S-(1-oxyl-2,2,5,5-tetramethyl-2,5-dihydro-1H-pyrrol-3-yl)methyl methanesulfonothioate) in the absence or presence of 2 mM ascorbic acid. Briefly, samples were prepared by dissolving lyophilized ^{15}N S87C αS in NMR buffer to a final concentration of 1.256 mM, upon which a 6 X molar excess of

DTT was added and the mixture was incubated on a room-temperature rocker in the dark for approximately 30 min before being loaded onto a 7 kDa MWCO Zeba spin desalting column (Thermo 89891). The concentration of eluted protein in NMR buffer was confirmed by A_{280} measurements using an extinction coefficient of 5600 M^{-1} cm^{-1} (Fusco *et al.,* 2017). MTSL was added at a 10 X molar excess and the protein mixture was incubated on a room-temperature rocker in the dark for four hours before being run through a Hiload 16/600 Superdex 200 column equilibrated with NMR buffer. The eluted protein was concentrated using a 10 kDa Amicon centrifugal filter unit and the final protein concentration was confirmed by A_{280} measurements using an extinction coefficient of 5600 M^{-1} cm^{-1} (Fusco *et al.,* 2017). NMR samples were prepared using freshly concentrated protein in 5 mm NMR tubes and paramagnetic relaxation enhancement rates were measured at 283K with d30 delays of (t_a) 4.1ms and (t_b) 10ms. The read-out HSQC experiments were recorded with 300 (t_1) and 2048 (t_2) complex points and spectral widths of 35.00 and 16.23 ppm for the ^{15}N and ^{1}H dimensions, respectively. Thirty-two scans were recorded with a recycle delay of 1 s. Ascorbic acid was added to each sample to reduce the MTSL spin label and the protein was incubated for 1 hr at 283K before the above NMR experiments were repeated. Γ_2 relaxation was calculated based on following equation, using peak intensities from the four HSQC spectra acquired for each sample: $\Gamma_2 = (1/(t_b-t_a))*(\ln[\{I_{reduced,tb}*I_{oxidized,ta}\}/\{I_{reduced,ta}*I_{oxidized,tb}\}])$, based on equation 5 from Iwahara *et al.* 2007.

2.4.4 Saturation Transfer Difference (STD) with αS oligomers

The binding of ATP and ATP-Mg to kinetically trapped αS oligomers was monitored using 1D STD/STR NMR experiments acquired at 283K and involving oligomer on-resonance saturation at -85.801 Hz and 2048 scans for STD experiments and off-resonance saturation at 40 ppm and 128 scans for Saturation Transfer Reference (STR) experiments, based on the 1D oligomer peak identification by Narayanan and Reif, 2005. The STD experiments thus monitor saturation transfer from αS oligomers to interacting ATP molecules. Both STD and STR experiments were acquired with spectral widths of 11.7057 ppm, 16 K points, transmitter frequency offsets of 4.700 ppm and 32 dummy scans. ATP or ATP-Mg was titrated into samples of either 68.5 μM αS oligomers, 50 μM oligomers or 50 μM monomers and binding isotherms were constructed based on the STD:STR ratio of ATP peaks at 8.09 ppm (for 50 μM samples) and 5.98 ppm. After multiplying these ratios by the sample ATP or ATP-Mg concentration, the values were normalized to 1600 μM additive and fitted to the one-site specific binding model in GraphPad Prism 8.4.2.

2.4.5 Transverse ^{15}N Amide Relaxation R_2 Experiments to Characterize WT αS Monomer-Fibril Interactions in the Presence of ATP and ATP-Mg

Changes in αS residue relaxation rates upon binding to mature, late-stage fibrils were monitored via transverse ^{15}N amide relaxation R_2 experiments involving fresh 250 μM αS monomers prepared in NMR buffer in the presence or absence of both 1.325 mM (5.4-fold molar excess) unlabeled WT α-Syn fibrils and 10 mM ATP or ATP-Mg. ^{15}N transverse relaxation rates (^{15}N-R_2) were measured using a pseudo 3D pulse sequence

with water flip-back, heat compensation and sensitivity enhancement. The total CPMG lengths were 313.36, 62.72, 94.08, 125.44, 156.88 and 188.18ms using a τ delay (half the time between 180º pulses) of 900 µs. Spectra were acquired with 2048 (t_2) and 300 (t_1) points, 32 scans and recycle delays of 1 s.

2.4.6 Pairwise Chemical Shift Projection Analysis

To assess whether the shifts of WT αS $^{1}H,^{15}N$ HSQC cross-peaks induced by 10 mM ATP are consistently in one relative direction, residue-specific displacement vectors similar to equation 4 from Ahmed *et al.* (2017) were defined, with “holo” and “apo” representing samples in the presence and absence of ATP, respectively. Cos theta angles between displacement vectors of generic residues *i* and *j* were computed through the normalized dot product as in equation 5 from Ahmed *et al.* (2017). Residue pairs with $\cos\theta_{ij}$ values greater than 0.97 were then visualized in a 140 X 140 matrix.

2.5 Thioflavin T Fluorescence

The effect of ATP and ATP analogs on both initial and late-stage αS aggregation was monitored by ThT fluorescence measurements of fresh, 300 µM monomeric αS protein samples prepared in ThT buffer in the absence or presence of additives. Stock samples were prepared in 1.5 mL Eppendorf tubes on ice before being aliquoted into each of four wells of black, Greiner half-volume, glass-bottomed 96-well plates containing one 3 mm glass bead per well. Sample wells contained a 110 µL solution, while blank wells and buffer dams contained 110 uL and 300 µL buffer, respectively. Plates were sealed with a plastic sheet as well as a lid and ThT fluorescence measurements were

recorded from the plate bottom on a BioTek Instruments Cytation 5 Cell Imaging Multi-Mode plate reader set with extended gain and excitation and emission at 448 and 482 nm. For experiments monitoring the entire ThT time profile, plates were incubated in the reader for 85 hours at 37 ºC with 30 s orbital shaking prior to each read, spaced six minutes apart. Data are reported as the average fluorescence of the four wells for each condition at each timepoint. For plateau experiments, after taking baseline initial readings every 3-5 min for 30 min with 30 s orbital shaking prior to each read, plates were placed in a 37 ºC shaker at 150 rpm for 72 hrs before being incubated in the 37 ºC reader for 20 additional hours at plateau, with measurements also taken every 3 min as before. Data are reported as the 20-hour average fluorescence reading for each well of each condition at plateau, with error bars representing the standard deviation of all well averages for each condition, calculated in GraphPad Prism 8.4.2.

2.6 Dynamic Light Scattering

Besides forming late-stage, β-sheet fibrils, αS can assemble into intermediately-sized, soluble aggregate species that are less readily detectable by ThT, therefore DLS was used to probe the effect of ATP and ATP analogs on these smaller species. The above plateau ThT samples were diluted 2:1 with ThT buffer and ultracentrifuged at 121968 X g and 4ºC for 35 min. The supernatant was used for DLS measurements in 40 µL low-volume plastic cuvettes (ZEN0040) and measured at 10 ºC using 5 runs and 12 measurements per run. DLS was performed using a Zetasizer Nano ZS Instrument (Malvern Instruments, Malvern, UK). Autocorrelation functions were accumulated for 20 min with 20 s per measurement and 120 s of pre-equilibration time, at an angle θ of 173°

and using a 4 mW He−Ne laser operating at a wavelength of 633 nm. The particle diameter detection limit was 0.3 nm−10 μm. The viscosity value for water was used in the analysis of all measurements.

2.7 Negative Stain Transmission Electron Microscopy

To validate the ThT results and confirm the presence of fibrils, the plateau ThT samples were diluted 20 X using milliQH_2O and 3-5 μL drops of the diluted mixtures were spotted on Formvar-coated Cu/Pd grids (Electron Microscopy Sciences, G200-CP and RT 15800) for 5-7 min. After blotting excess sample with filter paper, the grids were stained with equal volumes of 1% uranyl acetate for 1 min. Grids were loaded in a room-temperature holder and introduced into a JEOL 1200-EX electron microscope operated at 80 kV and imaged at 40,000 X direct magnification. All images were acquired with an AMT XR-41 side-mount cooled 4-megapixel format CCD camera.

2.8 Size Exclusion Chromatography Coupled with Multiangle Light Scattering

SEC-MALS measurements were conducted on a Wyatt miniDAWN MALS detector coupled to a Wyatt Optilab rEX online refractive index detector. Final 1D STD/STR NMR samples of approximately 68.57 μM αS oligomers in the presence of 1.6 mM ATP were diluted to 700 μL in 1X PBS, 100% D_20, pH 7.4 before being centrifuged at 14,000 X g for 2 min at 4 ºC. The top 650 μL of supernatant was removed into a new tube and 500 μL of this mixture was injected into a Superdex 200 increase 10/300 analytical gel filtration column (GE Healthcare) running at 0.4 mL/min in PBS buffer before passing through the light scattering and refractive index detectors in a standard SEC-MALS format.

2.9 Sodium Dodecyl-Sulfate Polyacrylamide Gel Electrophoresis (SDS-PAGE)

To analyze the effect of ATP on the relative amounts of low-molecular-weight (LMW), intermediate-molecular-weight (IMW) and high-molecular-weight aggregates of E46K and A53T αS, 500 µL aliquots from the aforementioned plateau ThT sample supernatants used for DLS were centrifuged at 14,000 X g for 20 min at 4 ºC using a Pall Nanostep 100 kDa centrifugal filter. The flow-through was designated the LMW sample. The retained material was resuspended in 50 µL ThT buffer as the IMW sample. The DLS ultracentrifuge pellet was resuspended in 100 µL milliQH_20 as the HMW sample. Each LMW and HMW sample was mixed at a 1:1:3 ratio with Laemmli buffer and ThT buffer, while each IMW sample was mixed at a 4:1 ratio with Laemmli buffer for SDS-PAGE. The IMW sample ratio was different from that for LMW and HMW samples to enable visualization of lowly-populated species on the gel. These samples were heated to >100ºC for 5 min and separated on an 18% SDS-PAGE gel at 150 V. Gels were stained for 10 min at room temperature following 30 s of heating, then de-stained overnight and imaged. To quantify the relative amounts of HMW versus LMW aggregates for each condition, the intensities of each monomer band at approximately 15 kDa were estimated in ImageJ and the HMW/LMW intensity ratios were calculated.

2.10 References

Ahmed, R., Huang, J., Weber, D.K., Gopinath, T., Veglia, G., Akimoto, M., Khondker, A., Rheinstädter, M.C., Huynh, V., Wylie, R.G., Bozelli Jr., J.C., Epand, R.M., and Melacini, G. (2020) Molecular mechanism for the suppression of alpha synuclein membrane toxicity by an unconventional extracellular chaperone. *J. Am. Chem. Soc. 142,* 9686-9699.

Ahmed, R., VanSchouwen, B., Jafari, N., Ni, X., Ortega, J., and Melacini, G. (2017) Molecular mechanism for the (−)-epigallocatechin gallate-induced toxic to nontoxic remodeling of aβ oligomers. *J. Am. Chem. Soc. 139,* 13720-13734.

Boulton, S., Akimoto, M., Selvaratnam, R., Bashiri, A., and Melacini, G. (2014) A tool set to map allosteric networks through the NMR chemical shift covariance analysis. *Sci. Rep-UK. 4,* https://doi.org/10.1038/srep07306.

Chen, S.W., Drakulic, S., Deas, E., Ouberai, M., Aprile, F.A., Arranz, R., Ness, S., Roodveldt, C., Guilliams, T., De-Genst, E.J., Klenerman, D., Wood, N.W., Knowles, T.P., Alfonso, C., Rivas, G., Abramov, A.Y., Valpuesta, J.M., Dobson, C.M., and Cremades, N. (2015) Structural characterization of toxic oligomers that are kinetically trapped during α-synuclein fibril formation. *PNAS. 112,* E1994-2003.

Fusco, G., Chen, S.W., Williamson, P.T.F., Cascella, R., Perni, M., Jarvis, J.A., Cecchi, C., Vendruscolo, M., Chiti, F., Cremades, N., Ying, L., Dobson, C.M., and De Simone, A. (2017) Structural basis of membrane disruption and cellular toxicity by α-synuclein oligomers. *Science. 358,* 1440-1443.

Hoyer, W., Antony, T., Cherny, D., Heim, G., Jovin, T.M., and Subramaniam, V. (2002) Dependence of alpha-synuclein aggregate morphology on solution conditions. *J. Mol. Biol. 322,* 383-393.

Iwahara, J., Tang, C., and Clore, G.M. (2007) Practical aspects of ^{1}H transverse paramagnetic relaxation enhancement measurements on macromolecules. *J. Magn. Reson. 184,* 185-195.

Kumari, P., Ghosh, D., Vanas, A., Fleischmann, Y., Wiegand, T., Jeschke, G., Riek, R., and Eichmann, C. (2021) Structural insights into α-synuclein monomer-fibril interactions. *PNAS. 118,* e2012171118.

Narayanan, S., and Reif, B. (2005) Characterization of chemical exchange between soluble and aggregated states of β-amyloid by solution-state NMR upon variation of salt conditions. *Biochemistry. 44,* 1444-1452.

Selvaratnam, R., Chowdhury, S., VanSchouwen, B., and Melacini, G. (2011) Mapping allostery through the covariance analysis of NMR chemical shifts. *PNAS. 108,* 6133-6138.

Shao, H., Boulton, S., Olivieri, C., Mohamed, H., Akimoto, M., Subrahmanian, M.V., Veglia, G., Markley, J.L., Melacini, G., and Lee, W. (2021) CHESPA/CHESCA-SPARKY: automated NMR data analysis plugins for SPARKY to map protein allostery. *Bioinformatics. 37,* 1176-1177.

Wördehoff, M.M., and Hoyer, W. (2018) α-Synuclein aggregation monitored by thioflavin T fluorescence assay. *Bio-protocol. 8,* DOI:10.21769/BioProtoc.2941.

Chapter 3

Results and Discussion for the Effect of ATP on WT αS

3.1 ATP Interacts Weakly-Specifically with the N-terminal Lys- and Thr-dense Pseudo-apolipoprotein-like Repeats in WT αS Monomers

As a first step towards identifying the driving mechanism behind the interaction of ATP with WT αS monomers, we measured the residue-specific αS chemical shifts induced by increasing concentrations of ATP, in the absence of salt, so as not to screen any potential charge-driven interactions. Figures 2a-c show that ATP induces modest but nonetheless significant, reproducible and concentration-dependent chemical shifts in primarily N-terminal lysine and threonine residues within the second, third, fourth and fifth of the nine total pseudo-apolipoprotein repeats of αS, leaving the lysine and threonine residues in the NAC and C-terminal imperfect “KTKEGV” repeats largely unaffected (Alza *et al.,* 2019; Dettmer *et al.,* 2015). This suggests that although ATP has an increased affinity for certain αS residues, the ATP-αS interaction is primarily driven by the high concentration of polar and positively-charged residues in the αS N-terminus. This conclusion is further supported by the $\cos\theta_{ij}$ matrix in Figure 2d as well as the residue-specific shifts in Figures 2a and b, which indicate that many residue pairs in particularly the NAC region, but also throughout residues 20 – 140 as well, experience ATP-induced chemical shift changes in the same general direction in the ^{15}N and ^{1}H plane. As highly specific binding typically induces chemical shifts in different directions, the parallel nature of many of the αS ATP-induced shifts suggests that ATP approaches in one consistent orientation to many different residues (Figure 2d) (Ahmed *et al.,* 2017). This suggests that

the mode of ATP binding is likely conserved, even between different residues whose side chains likely point in different directions (Ahmed *et al.,* 2017). Overall, the fact that ATP causes shifts in only certain threonine and lysine residues, when considered with the $\cos\theta_{ij}$ matrix results, indicates that the ATP-αS interaction is weakly specific (Figures 2a-d).

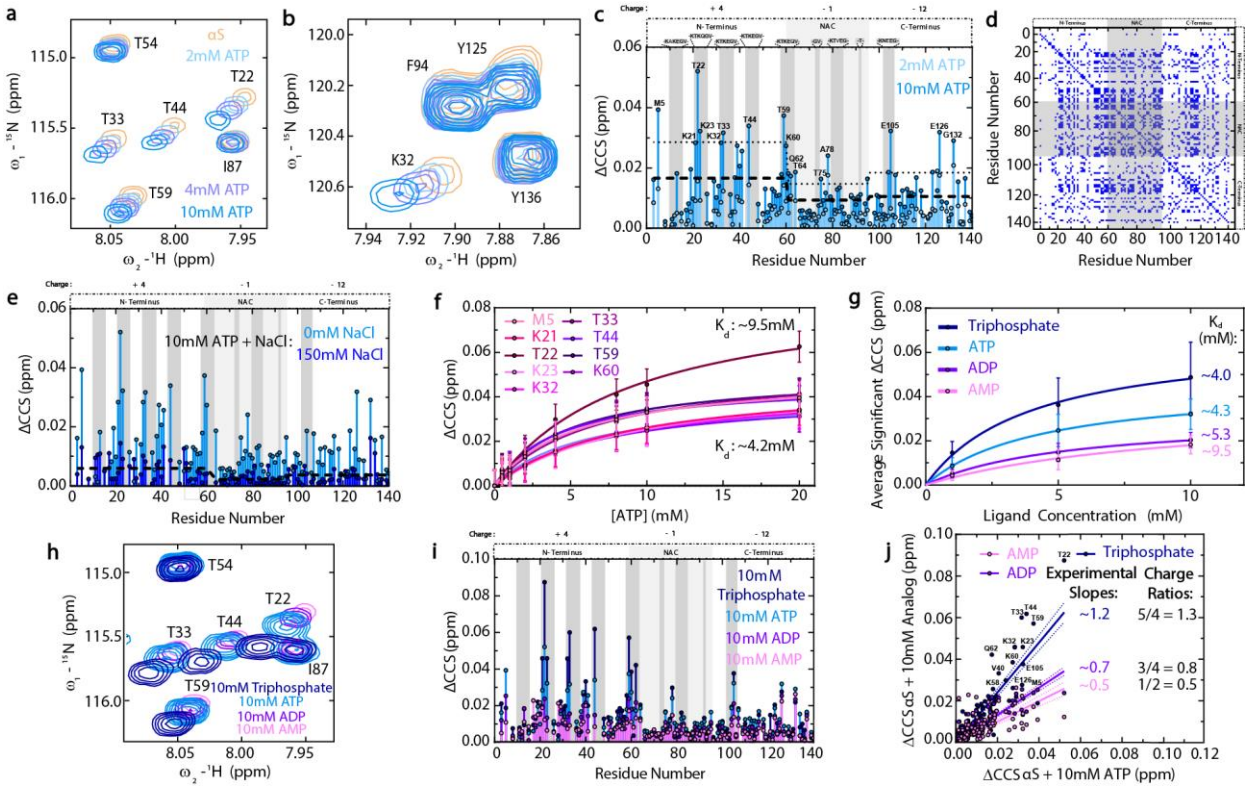

Figure 2. The triphosphate moiety of ATP drives its weak (~mM) electrostatic interaction with the Lys- and Thr-dense N-terminal pseudo-apolipoprotein repeats of WT αS monomers. (a and b) Representative zoomed-in expansions of ^{1}H-^{15}N HSQC spectra, colored as per legend in a. (c) Compounded chemical shift changes (ΔCCS) of αS in the presence of increasing concentrations of ATP. Residues with ΔCCS values greater than the region-specific average shift (dashed line) plus one standard deviation (dotted line) are labelled. (d) Cosθ matrix for αS WT ("apo") versus 10 mM ATP-bound αS WT ("holo"). A cutoff of cosθ > 0.97 was used to display the cross-peaks. (e) αS ΔCCS induced by 10 mM ATP

addition in the absence or presence of 150 mM NaCl. (f) ΔCCS of significantly-shifted N-terminal residues of αS titrated with 0-20 mM ATP, shown *vs.* ATP concentration and fitted to a one-site specific binding model. Shown are the lower and upper limit model-calculated residue approximate K_d values. Error bars are estimated as per method of Selvaratnam *et al.* (2011). (g) Average ΔCCS of significantly-shifted residues of αS titrated with AMP, ADP, ATP or Triphosphate, fitted to the one site specific binding model. Shown are approximate fitted K_d values. Error bars represent the standard deviation of all well-resolved αS residue peaks at a given additive concentration. (h) Zoomed-in region of overlayed ^{1}H-^{15}N HSQC spectra used to calculate panel g ΔCCS with labelled residues showing localization of phosphate-induced αS shifts to predominantly N-terminal threonine residues. (i) ΔCCS from ^{1}H-^{15}N HSQCs of αS titrated with 10 mM AMP, ADP, ATP or Triphosphate. The ATP-induced αS residue shifts are shown in e, h and i for ease of comparison. The charges of each labelled αS region are shown above panels c, e and i, with the dark grey boxes representing the imperfect pseudo-apolipoprotein "KTKEGV" αS repeats, the sequences of which are shown in panel c. (j) Correlations between residue-specific αS ΔCCS values induced by 10 mM ATP and ΔCCS values induced by 10 mM of either AMP, ADP or Triphosphate. Approximate slopes are shown with lines of best fit and error. Significantly shifted residues for Triphosphate are labelled. All figures were prepared in GraphPad Prism 8.4.2. and Adobe Illustrator 26.3.1., all significantly overlapped peaks were removed from the spectra and all ^{1}H-^{15}N Heteronuclear Single Quantum Coherence (HSQC) NMR experiments were acquired using fresh 120 µM WT ^{15}N αS in 50 mM Hepes, 5% D_20, pH 7.4 buffer on a Bruker AV 700 spectrometer at approximately 10ºC. ΔCCS are plotted versus αS residue number and calculated as $\Delta CCS = (0.5*((\delta H_{AMP,\ ADP,\ ATP\ or\ Triphosphate} - \delta H_{\alpha S})^2 + (0.15*(\delta N_{AMP,\ ADP,\ ATP\ or\ Triphosphate} - \delta N_{\alpha S})^2)))^{1/2}$ (Lautenschläger *et al.,* 2018).

Our ^{1}H-^{15}N HSQC analyses also rule out that the ATP-αS interaction is driven by the aromatic ring of ATP clustering over protein hydrophobic patches (Figure 1b, NAC region), since aromatic αS residues in the C-terminus and hydrophobic NAC region do not show significant, concentration-dependent chemical shifts (Figure 2b-c). However,

the modest, ATP-induced shifts in certain aromatic residues like Y125 do not rule out the possibility that there may be a small degree of π-π stacking interactions between aromatic residues of αS and the adenine ring of ATP, although the overall interaction between αS and ATP is not likely predominantly hydrophobic (Figure 2b). The few significantly-shifted C-terminal glycine and negatively-charged glutamic acid residues shown in Figure 2c are likely the result of residual sodium ions in the ATP formulation binding to the αS C-terminus, which has been shown to bind a variety of metal ions (Moons *et al.,* 2020). Given their isolated nature and scarcity, it is unlikely that these shifts report on the general driving mechanism of the ATP-αS interaction. Rather we hypothesize that the binding of ATP to αS is predominantly electrostatically-driven, given the preference of ATP to interact with polar and positively-charged residues within the positively-charged N-terminus of WT αS monomers.

3.2 The ATP-αS Interaction is Electrostatic and Weak but Still Biologically-Relevant

To confirm our hypothesis that the ATP-αS interaction is indeed primarily electrostatic, we next measured how αS residue-specific chemical shifts induced by 10 mM ATP are affected by 150 mM NaCl (Figure 2e). Figure 2e shows that 150 mM NaCl de-tunes but does not abolish the ATP-αS interaction, causing widespread reductions in the magnitude of the N-terminal, NAC and C-terminal ATP-induced αS chemical shifts, while maintaining the overall pattern of greatest ATP-induced N-terminal region-specific αS shifts. The salt-dependence of ATP-induced ppm changes and the consistent pattern of ATP inducing the most significant shifts in the αS N-terminus, even in the presence of NaCl, suggests that the ATP-αS interaction is predominantly electrostatically-driven.

To address whether the ATP-αS interaction is still biologically-relevant given its modulation by physiologically-relevant salt concentrations, we fitted the most significant, N-terminal residue-specific αS chemical shifts induced by 0-20 mM ATP to a one-site specific binding model and extracted approximate K_ds (Figure 2f) (Dang *et al.,* 2021). Interestingly, although these K_ds span a range from approximately 4.2 to 9.5 mM, suggesting a relatively weak interaction, they are nonetheless similar to the 3.77 ± 0.49 mM K_d for the specific binding of ATP to a pocket of FUS, a binding, moreover, that has a biologically-relevant effect on FUS solubility (Figure 2f) (Kang *et al.,* 2018). Given that the cellular ATP concentration ranges from 2-12 mM, it is reasonable to assume, therefore, that a significant proportion of ATP may be bound to αS *in vivo*, even in the presence of 150 mM NaCl (Dang *et al.,* 2021; He *et al.,* 2020). In addition, since the binding isotherms in Figure 2f appear to plateau/saturate, it is likely that the interaction between ATP and αS in cells has a certain level of specificity and is not, therefore, a completely general, non-specific interaction. Overall, the results in Figures 2e and f indicate that although the ATP-αS interaction is electrostatic, it is nonetheless specific and strong enough to be both biologically and pathologically-relevant (Dang *et al.,* 2021).

3.3 The Phosphate Groups of ATP Drive its Electrostatic Interaction with WT αS Monomers

Since the exact mechanism of how ATP interacts with a specific protein is essential to determining whether it has a hydrotropic or a pathological pro-aggregation effect, we compared the residue-specific αS chemical shifts induced by ATP to those induced by ATP analogs AMP, ADP and Triphosphate in order to determine whether the electrostatic

nature of the ATP-αS interaction is driven by the triphosphate moeity (Greiner and Glonek, 2020; Heo *et al.,* 2020). The results in Figure 2g indicate that the number of phosphate groups influences the ATP-αS interaction, since the average K_ds follow a consistent decreasing trend as the number of phosphate groups in the ATP analog increases. The N-terminal αS residue shifts induced by increasing concentrations of ATP follow a similar pattern to those induced by AMP, ADP and Triphosphate and target the same N-terminal threonines – 22, 33, 44 and 59 (Figure 2h and i) (Yamaguchi *et al.,* 2021). The correlations between the ATP-analog-induced and the ATP-induced αS chemical shifts also become closer to one as the number of phosphate group increases and, interestingly, the slopes of these correlations are quite similar to the ratio of charges between the ATP analogs and ATP at physiological pH 7 (Figure 2j). These results consistently suggest that the ATP-αS interaction is driven by the triphosphate moeity and is therefore predominantly electrostatic (Figure 2g-j) (Zhang *et al.,* 2017). Moreover, these results explain previous observations by Nishizawa *et al.* (2021), who showed that changing the nucleobase of ATP does not significantly affect its interaction with αS and that the effect of adenosine, which lacks the triphosphate moiety, is significantly different than that of ATP. Considering the relevance of the triphosphate, we hypothesized that Mg^{2+} complexation with the phosphates of ATP and the corresponding partial charge neutralization of the triphosphate moiety would influence the ATP-αS interaction under biologically-relevant conditions (Holm, 2012).

3.4 Magnesium Modulates the Interaction of ATP with αS Monomers and *Vice-Versa*

Since Mg^{2+} complexation is required for ATP's biological function as an energy source and Mg^{2+} levels decline with age and are often greatly reduced in PD patients, we next sought to characterize the effect of Mg^{2+} on the ATP-αS interaction by comparing the αS chemical shifts induced by ATP to those induced by ATP-Mg and $MgCl_2$ (Calamai *et al.,* 2006; Golts *et al.,* 2002; Yamanaka *et al.,* 2016). Consistent with our emerging model of ATP's phosphate groups driving its electrostatic interaction with predominantly the αS N-terminus, Figures 3a, b and e show that the complexation of Mg^{2+} with the triphosphate moeity of ATP attenuates to different extents the ATP-induced N-terminal αS shifts. At both the N- and C-termini of αS, the effect of ATP-Mg is intermediate between that of ATP and $MgCl_2$, suggesting that while Mg^{2+} complexation slightly de-tunes the interaction of ATP and αS, it does not entirely eliminate the ATP-αS interaction, even under more biologically-relevant conditions (Figure 3a-e) (Yamanaka *et al.,* 2016). Magnesium is therefore clearly able to influence the interaction of ATP and αS, but the results in Figure 3c-e also suggest that ATP is able to de-tune the significant binding of Mg^{2+} to the C-terminus of αS monomers. This suggests that the presence of ATP inhibits the binding of Mg^{2+} to the αS metal ion-binding site, which leads us to hypothesize that ATP is able to sequester Mg^{2+} away from αS and that, once bound to ATP and partially charge-neutralized, Mg^{2+} binds αS more weakly (Moons *et al.,* 2020).

To further explore this phenomenon, we then measured how the addition of increasing concentrations of ATP to Mg-bound αS affects the Mg-induced αS chemical shifts. The de-tuning effect of ATP on Mg^{2+} binding to αS is evident by the concentration-dependent decreases in the C-terminal Mg-induced αS chemical shifts in Figure 3f-h,

confirming that ATP is able to sequester Mg^{2+} away from αS monomers as ATP-Mg. The increasing formation of ATP-Mg as ATP is titrated into Mg-bound αS also accounts for the absence of increasing N-terminal ATP-induced αS residue shifts, even as more ATP is added to the system (Figure 3f, i-j). Conversely, Figure 3k shows that as increasing concentrations of Mg^{2+} are added to ATP-bound WT αS monomers, the N-terminal ATP-induced αS chemical shifts show concentration-dependent decreases that are not accompanied by increased C-terminal Mg-induced αS residue shifts, indicating that the de-tuning effect of ATP on Mg^{2+} binding to αS occurs reciprocally and that the sequestration of ATP by Mg^{2+} as ATP-Mg affects both ligands' ability to bind αS. Since magnesium is known to affect pathological αS aggregation, the dynamic interplay between ATP, Mg^{2+}, ATP-Mg and αS suggests that ATP could serve as a Mg^{2+} "sink," buffering its effects on αS (Golts *et al.,* 2002). However, since Mg^{2+} levels are significantly reduced in PD patients, it is interesting to speculate whether a muted de-tuning effect of Mg^{2+} on the ATP-αS interaction occurs in these individuals, making the effect of ATP on αS not just biologically- but particularly pathologically-relevant (Golts *et al.,* 2002).

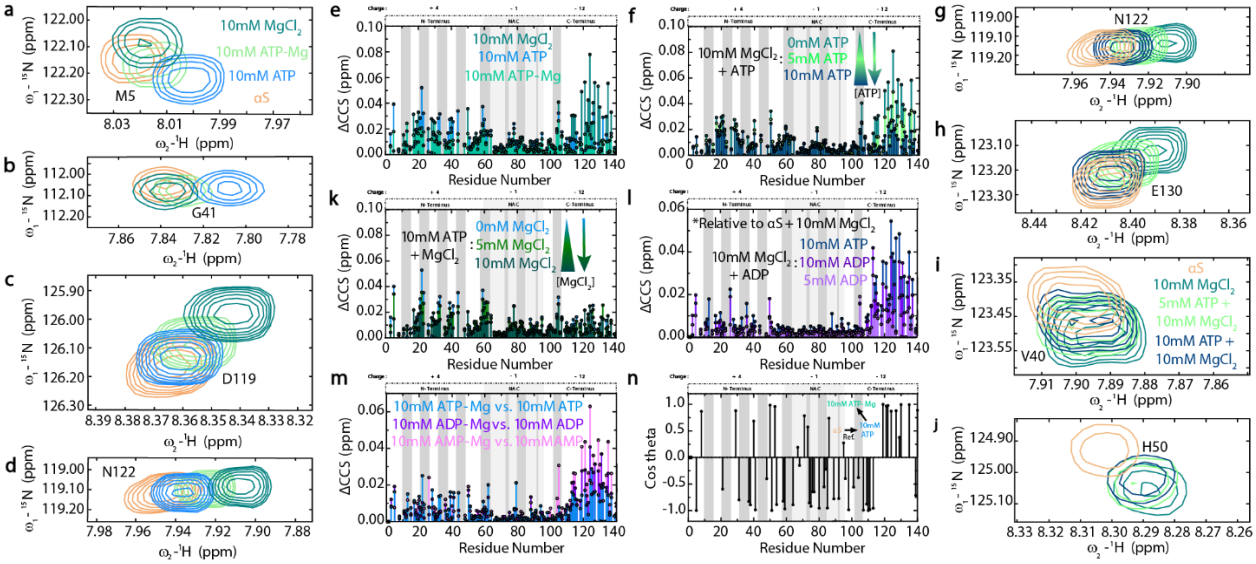

Figure 3. Magnesium modulates the interaction of ATP with αS monomers and *vice-versa*. (a-d) Zoomed-in regions of ^{1}H-^{15}N HSQC spectra of αS in the absence (brown) or presence of 10 mM ATP, ATP-Mg or $MgCl_2$, colored as per legend in a. (e) ΔCCS calculated from full spectra used to create panels a-d. (f) ΔCCS calculated from full ^{1}H-^{15}N HSQC spectra used to create panels g, h, i and j, showing αS pre-incubated overnight at 4 ºC in the presence of 10 mM $MgCl_2$ (teal) or with the subsequent addition of 5- or 10-mM ATP. Zoomed-in spectral regions in g, h, i and j are colored as per legend in panel i. (k) ΔCCS of αS induced by 10 mM ATP (blue) pre-incubated overnight at 4 ºC or with subsequent addition of 5 or 10 mM $MgCl_2$. (l) ΔCCS of αS pre-incubated overnight at 4 ºC in the presence of 10 mM $MgCl_2$ or with the subsequent addition of 5- or 10-mM ADP or 10 mM ATP. ΔCCS for this panel were calculated relative to αS + 10 mM $MgCl_2$: ΔCCS = (0.5*((δ$H_{ADP\ or\ ATP}$ – δ$H_{αS\ +\ 10\ mM\ MgCl2}$)^2 + (0.15*(δ$N_{ADP\ or\ ATP}$ – δ$N_{αS\ +\ 10\ mM\ MgCl2}$)^2)))^1/2 (Lautenschläger *et al.,* 2018). (m) Difference between ^{1}H-^{15}N HSQC-derived αS chemical shifts induced by 10 mM ATP-Mg and ATP (blue), ADP-Mg and ADP (purple) and AMP-Mg and AMP (pink). ΔCCS are plotted versus αS residue number and were calculated for panels e, f, k and m relative to αS. (n) Residue-specific cosθ profile from CHESPA analysis of 10 mM ATP-Mg binding to αS relative to αS and αS bound to 10 mM ATP, plotted versus αS residue number. The angle θ is that between the perturbation vector from αS and 10 mM ATP to αS and 10 mM ATP-Mg and the reference vector of αS to αS and 10 mM ATP. The cut-off used was 0.001 ppm and all values were calculated in NMRFAM Sparky. Spectra of αS in the absence or presence of 10 mM ATP from Fig. 2 are shown also in this figure for reference and ease of comparison. The charges of each labelled αS region are shown above the plots with the dark grey boxes representing the imperfect “KTKEGV” αS repeats. All figures were prepared in GraphPad Prism 8.4.2. and Adobe Illustrator 26.3.1., all significantly overlapped peaks were removed from the spectra and all ^{1}H-^{15}N HSQC NMR experiments were performed using fresh 120 µM WT ^{15}N αS in 50 mM Hepes, 5% D_20, pH 7.4 buffer on a Bruker AV 700 spectrometer at 10 ºC.

3.5 The Phosphate-Driven Sequestration of Mg^{2+} by ATP Leaves Residual Mg^{2+} to Bind the C-Terminus of αS Monomers while ATP Affects the N-Terminus and NAC Regions

To assess whether Mg^{2+} binding to the triphosphate moiety of ATP drives its de-tuning effect on the interaction between ATP and αS, we next measured the concentration-dependent αS chemical shifts induced by ADP versus ATP on Mg-bound αS. In addition to the fact that ADP is biologically-relevant as a breakdown product of ATP hydrolysis, our interest in the ADP-αS interaction is also based on the reduced ability of ADP's two phosphate groups to bind and sequester Mg^{2+} and whether or not this weakens the de-tuning effect of Mg^{2+} as compared to that involving ATP. Figures 3f and i-j suggest that the significant, C-terminal αS chemical shifts induced by ATP addition to Mg-bound αS, when considered relative to those induced by Mg^{2+}, report on the ability of ATP to sequester Mg^{2+} away from the αS C-terminus, causing these residues to shift toward an unbound state and therefore reversing the shifts induced by Mg^{2+} binding. As such, the results in Figure 3l suggest that ADP is less able to sequester Mg^{2+} than ATP, indicating that the sequestering effect is indeed due to phosphate-mediated Mg-binding. Figure 3l also shows that the concentration-dependent C-terminal αS residue shifts induced by ADP are not mirrored by increased N-terminal shifts. This observation indicates that, despite the reduced de-tuning effect of ADP on the αS-Mg^{2+} interaction, the reduced number of phosphate groups in ADP relative to ATP still hinders its association with the αS N-terminus. The phosphate groups are therefore key drivers of the ATP-αS interaction.

Although the idea that Mg^{2+} reduces the binding of ATP to proteins via a partial neutralization of ATP's strong anionic character has been suggested before (Nishizawa *et al.,* 2021), here we show that ATP is actually able to sequester Mg^{2+} away from αS and *vice versa*. Hence our emerging model of an electrostatic, phosphate-driven effect of ATP on primarily the N-terminus of αS somewhat differs from previous hypotheses suggesting that the significant C-terminal αS residue shifts caused by ATP addition to Mg-bound αS are indicative of Mg bridging ATP with primarily the αS C-terminus (Nishizawa *et al.,* 2021). It is possible that the Mg-sequestration and Mg-bridging models are not mutually exclusive and represent two viable mechanisms of ATP-αS interactions, one of which may prevail under diverse experimental conditions.

One key implication of the Mg-sequestration model is that ATP-Mg serves as a "buffer," controlling the amount of free ATP and Mg^{2+} available to interact with αS. To test this prediction and check whether residual free Mg^{2+} is sufficient to affect αS, even in the presence of ATP-analog "buffers", we measured the αS chemical shifts in solutions of AMP-Mg, ADP-Mg and ATP-Mg, relative to those induced by AMP, ADP or ATP alone (Yamanaka *et al.,* 2016). Indeed, we see a clear pattern of increasing, Mg-induced C-terminal αS chemical shifts caused by ATP-Mg, ADP-Mg and AMP-Mg, respectively, relative to the corresponding analog alone, suggesting that the decreasing number of phosphate groups in ATP, ADP and AMP leave consecutively more Mg^{2+} available to bind αS (Figure 3m). Interestingly, even with the ATP-Mg "buffer," residual free Mg^{2+} is likely available in cells to affect αS monomers, since we show that ATP is unable to chelate 100% of equimolar Mg^{2+} (Figure 3m). Furthermore, the significant and predominantly positive C-terminal cosθ CHESPA values in Figure 3n show that the addition of ATP-Mg

to αS monomers shifts the C-terminal region farther from the αS alone state relative to the ATP-bound state, suggesting that ATP-Mg is reinforcing an effect already present with ATP. This is likely the effect of Na^+ and Mg^{2+} cations, highlighting the fact that ATP is unable to chelate 100% of Mg^{2+}.

By contrast, the cosθ CHESPA values for the αS N-terminal and NAC regions are predominantly negative, suggesting that Mg^{2+} complexation with ATP shifts the N-terminus and NAC regions back toward the unbound state, consistent with our hypothesis of ATP-Mg sequestering ATP from αS (Figure 3n). We hypothesized that this effect of ATP on the NAC region of αS monomers could be indirect and due to a perturbation of long-range contacts between αS residues, which have been shown to expose the NAC region as the overall monomer conformation changes (Bisi *et al.,* 2021). To test this hypothesis, we next evaluated the effect of ATP on residue-specific Γ_2 relaxation rates of spin-labeled S87C αS monomers using intramolecular PRE experiments, which are exquisitely sensitive to changes in inter-residue distances caused by conformational changes (Karamanos *et al.,* 2015).

3.6 ATP Disrupts Long-Range Electrostatic Contacts in αS Monomers to Enhance Initial Aggregation

Our initial intramolecular PRE experiments characterizing the effect of ATP on residue-specific Γ_2 values of spin-labeled S87C αS monomers reveal that the addition of ATP causes widespread decreases in residue-specific Γ_2 values (Figure 4a). These decreases are particularly significant in the first 50 or so residues as well as in residues 110-140, indicating that these monomer regions are comparatively farther from the S87C

spin label in the presence of ATP than in untreated protein (Figure 4a). Since the PRE experiments report on the general closed/folded versus open/unfolded conformation of αS monomers, the Γ_2 losses suggest that the phosphate-driven targeting of ATP to the αS N-terminus and the corresponding partial charge neutralization disrupt long-range electrostatic contacts between the N- and C-termini of closed/folded αS monomers, causing the N- and C-termini of ATP-bound monomers to be farther from each other and the hydrophobic NAC region. Losses of such long-range electrostatic contacts in αS monomers have been shown to affect αS fibrillization kinetics, with an exposed NAC region driving increased aggregation (Bisi *et al.,* 2021). However, these PRE experiments do not, by themselves, confirm whether the ATP-mediated opening/unfolding of αS affects aggregation. Hence, we then used αS residue-specific intensity changes (Figure 4b) as well as differences in ThT fluorescence (Figure 4c) to evaluate whether the ATP-mediated disruption of long-range electrostatic contacts in αS monomers affects early aggregate formation.

Consistent with the significant ATP-induced Γ_2 losses at the αS N- and C-termini, the results in Figure 4b show an overall trend of intensity gains in αS residues 1 – 45 as well as 115 – 131, suggesting that the addition of ATP and its corresponding perturbation of stabilizing long-range N- and C-terminal contacts in αS monomers causes these regions to become more dynamic, with faster tumbling rates. By contrast, αS residues 48 to 114 show a clear trend of concentration-dependent intensity losses with ATP addition.

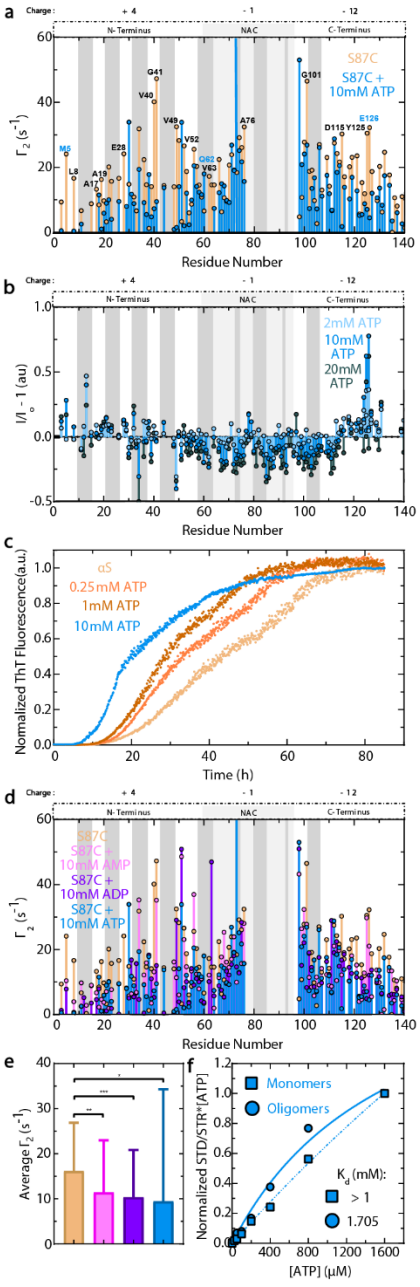

Figure 4. ATP disrupts long-range interactions between the N- and C-terminal regions of αS monomers in a phosphate-dependent manner and shortens the lag time for initial αS aggregation while interacting more strongly with oligomers. (a) Residue-specific Γ_2 values for spin-labeled, fresh 120 μM S87C ^{15}N αS in the absence (brown) or presence of 10 mM ATP. Residues with differences in Γ_2 values between the samples without and with ATP that are greater than region-specific averages plus one standard deviation are labeled. The blue-labeled residues also exhibit significantly shifted ppm values by 10 mM ATP (Fig. 2c). (b) Residue-specific HSQC intensity ratios of fresh 120 μM WT ^{15}N αS titrated with 2, 10 or 20 mM ATP relative to fresh 120 μM WT ^{15}N αS alone, and subtracting one. (c) Average ThT fluorescence measurements of fresh, 300 μM WT αS incubated with increasing concentrations of ATP in ThT buffer, as in Fig. 5, in a plate reader for 85 hours at 37 ºC with 30 s orbital shaking prior to each read (n=4). Data are normalized to the final measurement of αS alone. (d) Residue-specific Γ_2 values for spin-labeled, fresh 120 μM S87C ^{15}N αS in the absence (brown) or presence of 10 mM AMP, ADP or ATP. Panel e shows the average and standard deviation of all residues for each condition in panel d combined, colored as per legend in panel d. The average Γ_2 values in panel e were compared using an unpaired t-test with * representing 0.01 < p < 0.05, ** for 0.001 < p < 0.01 and *** for 0.0001 < p < 0.001. For panels a and d data for the 10 residues on either side of residue 87 are not shown, and the charges of each labelled αS region are shown above the plots with the dark grey boxes representing the imperfect “KTKEGV” αS repeats (the latter also shown in panel b). Residues with significant overlap or for which peaks entirely disappeared in one or more conditions are not shown. (f) Normalized 1D STD-based binding isotherms for the interaction of varying

concentrations of ATP with 50 μM of WT αS monomers (square, dashed line) or oligomers (circle, solid line). Values for ATP peaks at 8.09 ppm were fitted to the one-site specific binding model in GraphPad Prism 8.4.2. and are shown with the approximate model-calculated K_d values. All NMR experiments were performed using αS in 50 mM Hepes, 5% D_20, pH 7.4 buffer on a Bruker AV 700 spectrometer at approximately 10 ºC. All figures were prepared in GraphPad Prism 8.4.2 and Adobe Illustrator 26.3.1.

Since the perturbation of N- and C-terminal contacts in αS monomers has been shown to affect aggregation, we hypothesized that the ATP-induced intensity losses in Figure 4b could be reporting on the self-association of the NAC region to form a rigid fibril core (Bisi *et al.,* 2021). To test this hypothesis, we monitored WT αS aggregation over time in the presence of increasing ATP concentrations under physiologically-relevant salt and pH conditions (Figure 4c) (Dang *et al.,* 2021). Consistent with the ATP-induced αS residue-specific Γ_2 and NAC-region monomer intensity losses, the addition of increasing concentrations of ATP causes a concentration-dependent shortening of the lag time for initial αS aggregation (Figure 4c) (Golts *et al.,* 2002). Importantly, this effect is evident even at ATP concentrations as low as 0.25 and 1 mM, suggesting that the 2-12 mM ATP present in cells could enhance initial, pathologically-relevant αS aggregation *in vivo* (Figure 4c) (Dang *et al.,* 2021; Golts *et al.,* 2002).

3.7 The Disruption of αS Long-Range Electrostatic Contacts by ATP is Phosphate-Driven and Modulated by Magnesium

To gain insight into whether the perturbation effect of ATP on αS N- and C-terminal contacts is also driven by the triphosphate moeity, we next compared the effect of ATP on αS residue Γ_2 relaxation rates to those induced by AMP and ADP using intramolecular

PRE experiments. In addition to comparing the residue-specific changes in Γ_2, we also compared the effects of ATP analogs on average Γ_2 values from the entire αS sequence (Figure 4d and e). The latter show a clear trend of decreasing average Γ_2 with increasing number of phosphate groups (Figure 4e). The average Γ_2 values induced by AMP, ADP and ATP are also all significantly different than that of S87C αS alone (Figure 4e). Thus, the ATP-mediated disruption of long-range electrostatic contacts in αS monomers appears to be significant and phosphate-driven, paralleling the trend of increased interactions between AMP, ADP and ATP, respectively, and αS monomers (Figure 2g). Consistent with this hypothesis is the effect of ATP-Mg, which causes a significant decrease in the average Γ_2 value of S87C αS monomers that is greater than that caused by $MgCl_2$ but still less than that caused by ATP, indicating that the complexation of Mg^{2+} with the triphosphate moeity attenuates, but does not abolish, the significant effect of ATP on the overall conformation of αS monomers (Supplementary Figure 1a and b). Overall, these data suggest that the phosphate-driven interaction between ATP and primarily the N-terminus of αS monomers causes a partial neutralization of intrinsic αS charges that then disrupts the long-range N- and C-terminal contacts and causes monomer conformational changes. Therefore, the ATP-mediated enhancement of initial αS aggregation is likely a direct result of ATP binding, rather than a general, non-specific effect on the protein's hydration shell or an ATP-mediated alteration of solution properties, e.g., ionic strength or pH.

3.8 ATP Interacts Specifically and More Strongly with αS Oligomers

Having established the mechanism driving the interaction of ATP with WT αS monomers, we next aimed to characterize whether ATP also interacts with αS oligomers, since these are the primary neurotoxic αS species (Alza *et al.,* 2019). Thus, we prepared WT αS oligomers with a size greater than 50 kDa and characterized these by SEC-MALS before titrating them with ATP (Supplementary Figure 2). Binding isotherms constructed from 1D STD NMR experiments based on the signal saturation transfer from αS oligomers to ATP are consistent with a mM affinity (Figure 4f). The dissociation constant for the ATP-oligomer interaction is also slightly lower than the dissociation constant for the ATP-monomer interaction, which is slightly weaker and less specific (Figures 4f). Overall, this data suggests that the interaction of ATP with αS oligomers could be explained by the model for an electrostatically-driven interaction between negatively-charged polyelectrolytes and proteins proposed by Calamai *et al.* (2006). According to Calamai, positively-charged protein aggregates exhibit a greater concentration of charges than individual monomers and are therefore able to more strongly attract polyanions like DNA, ATP and heparin. The preferential ATP-oligomer interaction is also similar to that involving polyphosphates, which bind αS oligomers over monomers to alter their cytotoxicity (Lempart *et al.,* 2019). Therefore, it is interesting to speculate whether ATP is also able to modulate the PD-relevant cytotoxicity of αS oligomers by changing their structure (Lempart *et al.,* 2019).

3.9 ATP Inhibits Late-stage αS Cross β-sheet Fibril Formation at Plateau in a Phosphate-Dependent Manner that is Distinct from Salting-in or Salting-out Effects

Knowing that ATP enhances initial αS aggregation, we next studied the effect of ATP on late-stage αS aggregation by measuring plateau ThT fluorescence and imaging samples by TEM to assess whether the ATP-mediated increase in initial αS aggregation is accompanied by a similar increase in pathologically-relevant cross β-sheet fibril formation (Kumari *et al.,* 2021). In stark contrast to the pro-aggregation effect of ATP on initial αS aggregation, the results in Figure 5a show that ATP causes a dramatic and significant reduction in plateau ThT fluorescence that is clearly reflected by a reduced number of fibrils visible in the TEM images of the same samples (Figure 5c and d). The inhibition of αS cross β-sheet fibril formation by ATP is moreover not a non-specific salting-out or salting-in effect, as the ATP-mediated reduction in plateau ThT fluorescence is significantly different from the effects of ammonium sulfate and guanidine hydrochloride, which are at opposite ends of the Hofmeister series (Figure 5a). Thus, ATP is able to inhibit late-stage αS aggregation in a specific manner that is likely also phosphate-driven, since the complexation of Mg2+ with ATP attenuates the ATP-mediated effect, causing instead a significant enhancement of αS cross β-sheet fibril formation (Figure 5a and e) (Kumari *et al.,* 2021). This effect suggests that the interaction of ATP-Mg and αS, while less than that involving ATP, is nonetheless significant enough to affect pathologically-relevant aggregation (Figure 5a and e) (Golts *et al.,* 2002). Interestingly though, both ATP-Mg and ATP reduce the formation of soluble, intermediately-sized αS aggregates at plateau, an effect that is not recapitulated by MgCl2 (Supplementary Figure 3). Given the aforementioned TEM and ThT data (Figures

5a, c-e), this reduction suggests potentially different mechanisms-of-action of ATP and ATP-Mg on αS aggregation: while ATP inhibits aggregation by shifting the population of αS towards low-molecular-weight species, reducing the relative amount of both intermediately- and large-sized aggregates, ATP-Mg increases the conversion of intermediately-sized aggregates into large, fibrillar αS aggregates (Figures 5a, c-e and Supplementary Figure 3).

Our next step was to test whether the effect of ATP on late-stage αS aggregation is directly driven by the triphosphate moiety. To do this, we compared the plateau ThT fluorescence values of αS incubated with ATP analogs AMP, ADP and triphosphate to that induced by ATP (Figure 5b). The results in Figure 5b do show not only that the inhibition effect of ATP is phosphate-driven, but that it requires two or more phosphate groups, as AMP alone does not cause a significant reduction in ThT fluorescence of αS at plateau. Interestingly too, the dramatic reduction in late-stage αS fibril formation induced by ADP and ATP is slightly – but still significantly – greater than that induced by triphosphate, suggesting that the bulky adenosine group aids in inhibiting fibril formation (Figure 5b). Nevertheless, the significantly different effects of AMP versus ADP and ATP suggest that the bulk amount of negative phosphate charges is a key factor in driving the reduction in late-stage αS aggregation. The importance of two or more phosphate groups for driving a significant charge-driven effect of ATP on αS fibril formation is also similar to the mechanism of action of polyphosphates (Yamaguchi *et al.,* 2021). However, the net effect is quite different (Yamaguchi *et al.,* 2021). Whereas for tri-polyphosphate, the αS plateau ThT fluorescence has one maximum at ~10 mM, we report a dramatic reduction in αS plateau ThT fluorescence at an equivalent concentration of ATP (Figure 5a)

(Yamaguchi *et al.,* 2021). Thus, although the interaction mechanisms of αS with ATP and tri-polyphosphate are similar, it is unlikely that the effect of ATP on αS fibril formation can be described by the model proposed for polyphosphates, which involves charge-charge interactions enhancing low salt αS fibril formation (Yamaguchi *et al.,* 2021).

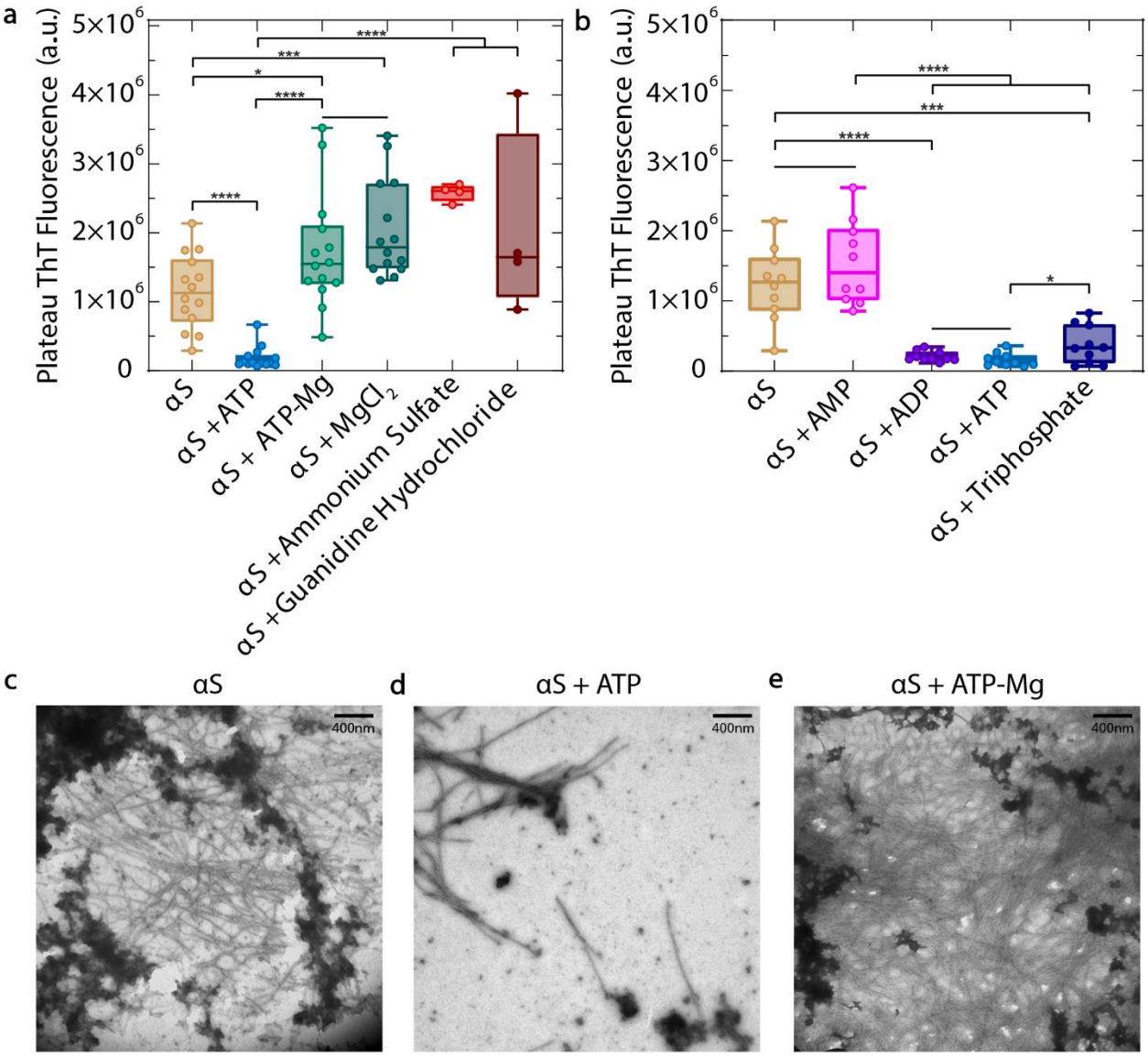

Figure 5. ATP inhibits late-stage αS cross β-sheet fibril formation at plateau in a phosphate-dependent manner that is distinct from salting-in or salting-out effects. (a and b) ThT fluorescence of fresh 300 μM WT αS in ThT buffer (20 mM K_2HPO_4, 5 mM KH_2PO_4, 100 mM KCl, 200 μM EDTA, 0.05%

NaN_3), incubated for 72 hrs in a 37 ºC shaker at 150 rpm before being incubated in a plate reader for 20 additional hours at plateau. Plotted are well-specific averages of ThT measurements from multiple separate experiments, taken at plateau every 5 min with 30 s orbital shaking prior to each read. Shown are αS in the absence or presence of (a) 10 mM ATP, ATP-Mg, $MgCl_2$, ammonium sulfate or guanidine hydrochloride, and (b) 10 mM AMP, ADP, ATP (for comparison) and Triphosphate. Average ThT values for each condition are compared using an unpaired t-test, with * for $0.01 < p < 0.05$, *** for $0.0001 < p < 0.001$ and **** for $p < 0.0001$. A flat line without * indicates no significant difference between treatments. (c, d and e) Negative stain transmission electron microscopy images of pelleted large aggregates from select panel a samples at plateau: αS alone (c) or in the presence of (d) 10 mM ATP or (e) 10 mM ATP-Mg. All scale bars represent lengths of 400 nm. Figures were prepared in GraphPad Prism 8.4.2. and Adobe Illustrator 26.3.1.

Consequently, we hypothesized that ATP binding to the N-terminus of αS monomers and the corresponding charge neutralization may specifically inhibit electrostatically-driven monomer-fibril interactions and secondary nucleation.

3.10 ATP Inhibits the N-terminally-driven Interaction Between αS Monomers and Fibrils

To check whether ATP affects the ability of bound αS monomers to interact with mature fibrils, we measured residue-specific transverse ^{15}N αS R_2 amide relaxation parameters induced by late-stage WT αS amyloid fibrils in both the absence and presence of ATP. As previously shown, we see systematic increases in R_2 rates throughout the N-terminus of ^{15}N αS monomers in the presence of mature fibrils (Figure 6a) (Kumari *et al.,* 2021). The model proposed by Kumari *et al.* (2021) suggests that these increases result from the positively-charged N-terminus of αS monomers binding to the exposed, highly-negatively-charged C-terminus of monomers present in fibrils and that this then is the

mechanism by which fibrils induce αS secondary nucleation. Given this hypothesis, it is particularly interesting and pathologically-relevant that we see decreases in N-terminal R_2 rates with ATP addition in the presence of fibrils that are not present in the absence of fibrils (Figure 6a). In fact, the general effect of ATP in the presence of fibrils is a widespread decrease in R_2 rates that, while most significant in the N-terminus, extends throughout the entire αS sequence (Figure 6b). Overall, these data suggest that ATP inhibits interactions between αS monomers and fibrils, particularly at the monomer N-terminus. Since the αS monomer-fibril interactions are predominantly electrostatic, it is likely that the muted interactions in the presence of ATP are due to ATP's N-terminal binding and positive-charge neutralization of αS monomers (Kumari *et al.,* 2021). In addition, the proposed π-π interactions between ATP and αS monomers likely compete with those that are critically important for monomer-fibril interactions (Kumari *et al.,* 2021). Given that ATP also inhibits αS cross β-sheet fibril formation at plateau, while still allowing the formation of some fibrils, it is particularly interesting to speculate whether the decrease in αS fibril amount in the presence of ATP relative to αS alone is due to ATP inhibiting monomer-fibril interactions and therefore suppressing secondary nucleation and its associated enhancement of αS aggregation.

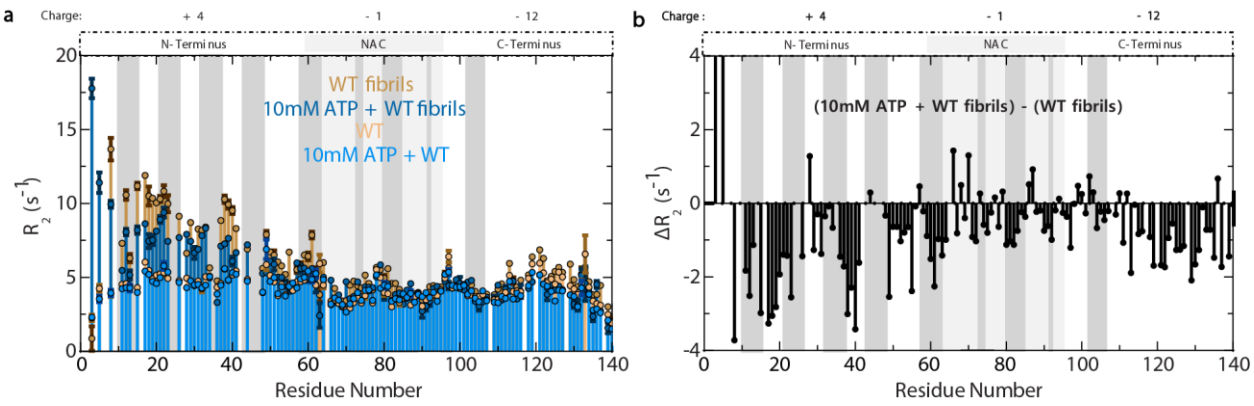

Figure 6. ATP inhibits the N-terminally-driven interaction between αS monomers and fibrils. (a) ^{15}N-R_2 profiles of 250 μM WT αS monomers in the absence (light brown) or presence (dark brown) of 1.3 mM WT fibrils (corresponding to an equivalent monomer αS concentration) as well as the presence of 10 mM ATP (blue) under both conditions. (b) Differences in R_2 values between the sample containing WT fibrils plus ATP and the sample of WT fibrils without ATP, calculated based on the samples in panel a. All figures were prepared in GraphPad Prism 8.4.2. and Adobe Illustrator 26.3.1., all significantly overlapped peaks were removed from the spectra and all NMR experiments were performed using fresh WT ^{15}N αS monomers in 50 mM Hepes, 5% D_20, pH 7.4 buffer on a Bruker AV 700 spectrometer at 10 ºC.

3.11 Proposed model to explain how the ATP-αS interaction influences αS aggregation

A persistent theme throughout this study is that the interaction between ATP and αS, though similar in some respects to published models describing the lysine-driven, electrostatic interaction between ATP and other amyloid proteins like Tau, displays unique features that we believe make it distinct from other published interactions involving ATP (Heo *et al.,* 2020). Our results identify the triphosphate moiety as the key driver of the electrostatic interaction between ATP and primarily lysine and threonine residues within the N-terminal pseudo-apolipoprotein-like repeats of αS monomers, thus

establishing that the ATP-αS interaction is similar to that between αS and polyphosphates (Figure 7) (Yamaguchi *et al.,* 2021). Nevertheless, here we show that such phosphate-driven ATP-protein interactions cause monomer conformational changes by direct binding, rather than by indirectly affecting the protein's hydration shell or by bridging/isolating monomers (Figure 7) (Greiner and Glonek, 2020; Heo *et al.,* 2020; Song, 2021). In addition, we show in detail the complex mutual interplay between Mg^{2+} and ATP and how it affects ATP-protein interactions. Since αS binds and is conformationally-affected by both ATP and Mg^{2+}, it presents a unique case in that Mg-complexation with ATP modulates the ATP-protein interaction and *vice versa*, with ATP-Mg serving as a "buffer" for the effects of both ligands on αS (Figure 3). Given the connection between Mg^{2+} levels and PD as well as the fact that ATP levels decline with age and aging is the greatest risk factor for PD, it is particularly interesting to speculate how this newly characterized interplay between ATP, Mg^{2+} and αS might influence disease development (Chaudhari and Kipreos, 2018; Golts *et al.,* 2002; Reeve *et al.,* 2014). In addition, since we show that ATP and Mg^{2+} both affect pathologically-relevant αS aggregation, this interplay becomes increasingly significant (Figures 5 and 8).

The effect of ATP on both early- and late-stage αS aggregation is perhaps the most unique feature of the interaction. Although a dual effect of ATP on protein solubility has been reported before in the case of FUS LLPS (Kang *et al.,* 2018), here we show a dual effect of ATP on protein aggregation, whereby the enhancement of initial αS aggregation via an ATP-dependent shortening of lag time occurs at the same ATP concentration as does the ATP-dependent inhibition of αS fibril formation.

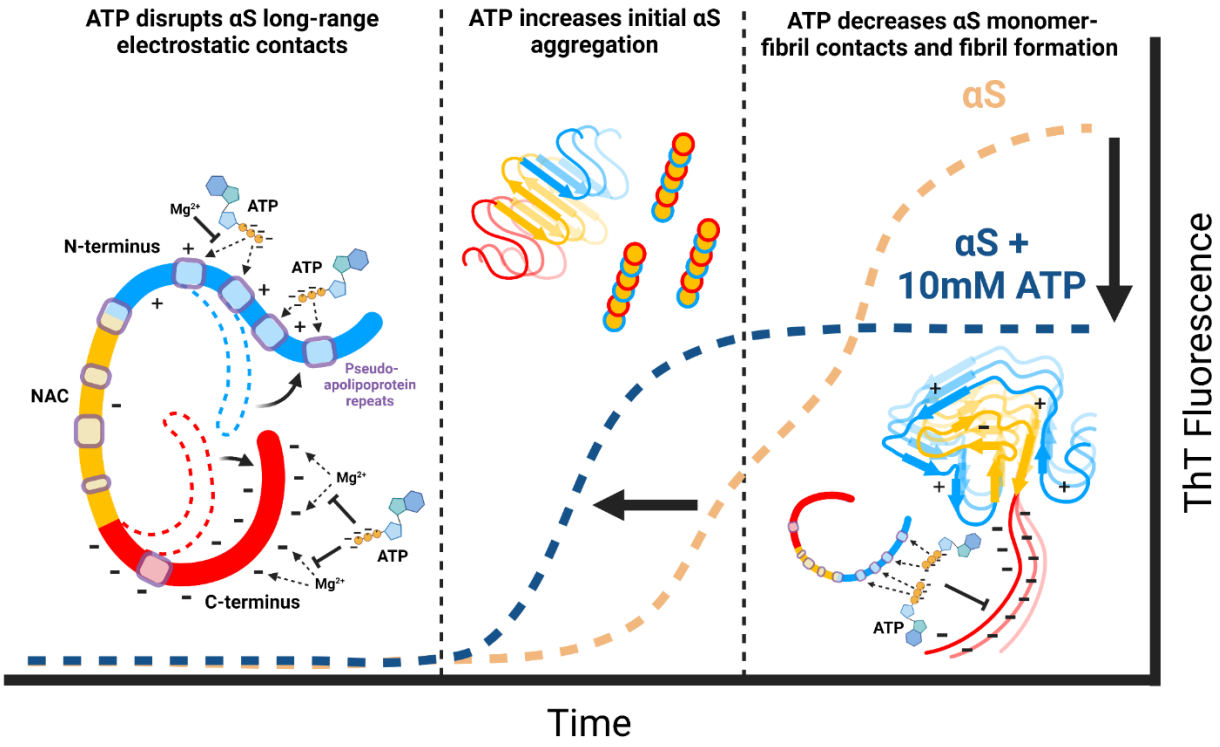

Figure 7. Proposed model to explain how the ATP-αS interaction influences αS aggregation. The triphosphate moiety of ATP targets primarily the Lys-dense pseudo-apolipoprotein-like repeats in the N-terminus of αS monomers in an electrostatically-driven interaction that is modulated by magnesium and which disrupts the electrostatic contacts between the N- and C-termini of αS monomers to cause unfolding and enhance early aggregate formation. ATP also interacts strongly with αS oligomers in a manner modulated by magnesium and suppresses the formation of intermediately-sized aggregates, both in the absence and presence of magnesium. Finally, ATP attenuates the N-terminally-driven interaction between αS monomers and fibrils to inhibit β-sheet fibril formation. Figure prepared in Biorender.

Our thorough characterization of the phosphate-driven effect of ATP on late-stage αS aggregation, moreover, points to a distinct mechanism by which ATP exerts a hydrotropic effect on amyloid aggregation that is uniquely evident only with ATP analogs containing two or more phosphate groups. If the inhibition of αS monomer-fibril contacts

by ATP does indeed suppress secondary nucleation, it is interesting to speculate how ATP modulates the prion-like spread of PD pathology since it potentially limits the ability of fibrils to seed new aggregates.

Chapter 4

Results and Discussion for the Effect of ATP on PD-Related αS Variants E46K and A53T

4.1 PD-related Mutations E46K and A53T Alter the Effect of ATP on αS Monomers

As a next step, we aimed to characterize how the effect of ATP on αS is influenced by the presence of common, PD-related point mutations E46K and A53T. To do this, we first measured the residue-specific chemical shifts induced by 10 mM ATP on WT, E46K and A53T αS monomers relative to the corresponding variant protein alone. Thus, these chemical shifts report primarily on the relative effects of ATP in the presence of αS mutations, rather than the effects of the mutations themselves, which are well known. Figure 8a shows that the effect of 10 mM ATP on A53T αS chemical shifts is quite similar to its effect on WT. This is consistent with the intensity ratios in Figure 8b, which show that although the magnitude of the ATP-induced intensity losses in particularly the beginning of the C-terminus are greater in the presence of A53T αS relative to WT, the overall patterns in the N-terminal and NAC regions are quite similar between A53T and WT. However, the overall pattern of ATP-induced intensity gains in residues 130-140 for WT is different than the intensity losses for A53T, suggesting perhaps that ATP has an altered affect on A53T αS monomer conformation and dynamics (Figure 8b). Taken together, these results suggest that even though the residue-specific effect, or binding, of ATP to A53T αS is similar to WT, ATP is nonetheless able to cause slightly increased self-association of the A53T αS NAC region, potentially leading to increased fibril core formation and altered aggregation kinetics.

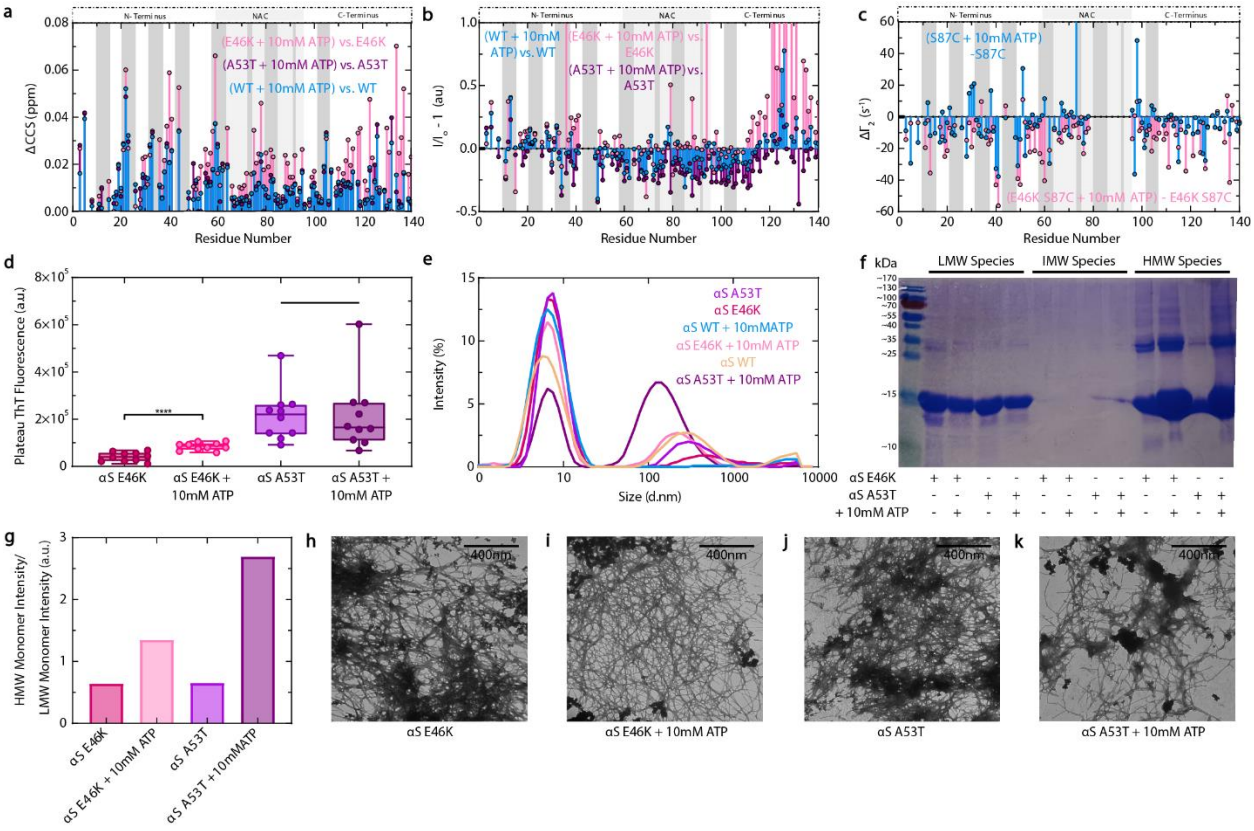

Figure 8. ATP promotes high-molecular-weight oligomer formation of E46K and A53T αS PD-related variants through mechanisms different from WT. (a) ^{1}H-^{15}N HSQC-derived compounded chemical shift changes of fresh, 120 μM ^{15}N WT (blue), E46K (pink) and A53T (purple) αS induced by 10 mM ATP, calculated relative to the corresponding variant alone. (b) Residue-specific ^{1}H-^{15}N HSQC intensity ratios of fresh, 120 μM ^{15}N WT (blue), E46K (pink) and A53T (purple) αS in the presence of 10 mM ATP, relative to the corresponding variant alone and subtracting one. (c) Differences in residue-specific Γ_2 values induced by 10 mM ATP and measured by intramolecular PREs experiments using spin-labeled, fresh 120 μM S87C ^{15}N (blue) or S87C E46K (pink) αS, calculated relative to the corresponding S87C variant alone. The ten residues on either side of 87 are not shown. Values for panels a, b and c are plotted relative to the αS residue number and labelled with the three αS regions as well as the nine, imperfect “KTKEGV” repeats, indicated by dark grey boxes. (d) Plateau ThT fluorescence measurements of fresh 300 μM E46K (pink) or A53T (purple) αS in ThT buffer, incubated as for Figures 5a and b. Plotted are well-specific averages of ThT measurements from multiple separate experiments, taken at plateau every 5 min with 30 s orbital

shaking prior to each read. Shown are αS variants in the absence or presence of 10 mM ATP (darker pink and purple, respectively). Average ThT values for each condition are compared using an unpaired t-test, with **** representing $p < 0.0001$. A flat line without * indicates no significant difference between treatments. (e) DLS intensity measurements of soluble αS recovered from panel d samples at plateau and following centrifugation to pellet large aggregates. (f) SDS-PAGE of soluble αS recovered from panel d samples following centrifugation that were subsequently either retained by (IMW) or passed through (LMW) a Pall Nanostep 100 kDa centrifugal filter. Resuspended centrifugation pellets constitute HMW samples. Bands are in reference to PageRuler Prestained Protein Ladder (26616, Thermo Scientific), shown in the left-most lane. (g) Quantification of panel f ~15 kDa monomer band intensities by ImageJ, expressed as the ratio of the HMW/LMW lane monomer bands for each sample. (h, i, j and k) Negative stain transmission electron microscopy images of pelleted large aggregates from panel d samples at plateau: E46K (h) or A53T (j) αS alone or in the presence of 10 mM ATP (i and k). All scale bars represent lengths of 400 nm. Figures were prepared in GraphPad Prism 8.4.2. and Adobe Illustrator 26.3.1.

By contrast, the residue-specific effect of ATP on E46K αS is extremely pronounced relative to WT, with significant chemical shift as well as intensity changes occurring throughout the αS sequence (Figure 8a and b). Interestingly, these differences appear most significant at the C-terminus of monomeric E46K αS, which shows particularly large intensity gains (Figure 8b). Unlike for WT αS, however, ATP does not cause major intensity losses throughout the NAC region for E46K monomers (Figure 8b). It appears, therefore, that the interaction between ATP and αS monomers is more significant in the presence of the PD-related E46K mutation, and that it has a different effect on monomer dynamics. While for WT αS, ATP causes self-association of the NAC region to eventually form a rigid fibril core, ATP enhances the dynamics of the C-terminus in E46K αS (Figure 8b). From this, we hypothesized that ATP binding to E46K αS might

cause increased disruption of the long-range electrostatic N- to C-terminal contacts that stabilize αS monomers and that this results in widespread changes in overall monomer conformation that lead to the significant chemical shifts and intensity gains shown in Figure 8a and b. To test this hypothesis, we performed intramolecular PRE experiments on S87C E46K αS monomers in the absence and presence of ATP (Figure 8c). Consistent with our hypothesis, we see greater differences in residue-specific Γ_2 values caused by ATP at both the N- and C-termini for E46K αS monomers relative to WT, suggesting that ATP causes a more significant disruption of long-range electrostatic contacts in αS monomers in the presence of the PD-related E46K mutation (Figure 8c). Given our overall model of the ATP-αS interaction being electrostatic and driven by the triphosphate moiety specifically binding to lysine and threonine residues, these results may indicate that the presence of an additional positive charge in the αS N-terminus caused by the E46K mutation leads to an enhanced interaction with ATP that then causes more significant N-terminal charge neutralization and overall monomer conformational changes. The latter result is also particularly interesting given that E46K αS monomers have enhanced N- to C-terminal electrostatic contacts (Bisi *et al.,* 2021). Thus, the ATP-αS interaction appears strong enough to overcome these enhanced contacts. As aforementioned, such changes likely lead to enhanced αS aggregation.

4.2 PD-related Mutations E46K and A53T Alter the Effect of ATP on αS Aggregates

To assess whether the residue-specific effects of ATP on E46K and A53T αS monomers lead to altered, pathologically-relevant aggregation, we next measured ThT fluorescence of E46K and A53T αS in the absence and presence of 10 mM ATP at plateau

and analyzed the aggregated species by DLS, SDS-PAGE and TEM. Figure 8d shows that, contrary to the results in Figure 5a showing dramatically decreased plateau ThT fluorescence of WT αS caused by ATP, ATP in the presence of E46K αS actually causes a significant enhancement of plateau ThT fluorescence relative to E46K αS alone. This suggests that ATP causes enhanced de-shielding of the E46K αS aggregation-prone NAC region. Taken together, the results in Figure 8a – d indicate that the presence of the PD-related E46K αS mutation does not just alter, but actually completely reverses, the effect of ATP on αS at plateau, changing it from inhibitory to enhancing. By contrast, the effect of ATP on A53T αS plateau ThT fluorescence is not significant, suggesting nonetheless that the A53T mutation attenuates the inhibitory ability of ATP on αS at plateau (Figure 8d). Instead, ATP shifts the population of soluble A53T αS away from small, low-molecular-weight species towards intermediately-sized and high-molecular-weight aggregates in a manner distinct from its effect on WT (Figures 7e – g). Whereas for WT αS ATP increases the relative amount of small, soluble species and eliminates the DLS peak caused by intermediately-sized, soluble aggregates, the A53T mutation causes it to have the opposite effect (Figure 8e). This then suggests that the significant NAC-region intensity losses in A53T αS monomers caused by ATP likely report on the formation of soluble aggregates that are not detected by ThT (Figures 7b,d,e). These aggregates are likely structurally different from the β-sheet-rich amyloid fibrils to which ThT normally binds, a conclusion that is supported by the slightly different average size of the intermediate-sized ATP-induced A53T αS aggregates relative to WT (Figure 8e). It is interesting to speculate whether ATP in the presence of A53T αS leads to the formation of amorphous aggregates that might have altered, PD-relevant cytotoxicity. Although

E46K αS is distinct from A53T in that it exhibits enhanced ATP-induced plateau ThT fluorescence, it too shows an increase in the relative amount of ATP-induced soluble, intermediately-sized aggregates with a slightly different average size than those produced in the absence of ATP (Figure 8d and e). Thus, the E46K and A53T αS mutations are similar in that they shift the population of soluble αS species towards higher molecular weights in the presence of ATP, while still allowing the formation of some fibrils (Figure 8f – k). Overall, these results suggest that the E46K and A53T mutations alter the effect of ATP on the aggregation pathway of αS in a manner that could potentially affect cytotoxicity and therefore PD-relevant pathology.

4.3 Relevance of ATP to E46K and A53T αS PD-related Pathology

Among the most significant findings of this study are the similar – and yet distinct – effects of ATP on PD-related αS variants E46K and A53T (Stephens *et al.,* 2020). For both of these proteins, ATP causes a unique shift towards intermediately-sized soluble aggregates that is not present for WT αS, suggesting perhaps that ATP increases the formation of pathologically-relevant oligomers of E46K and A53T αS (Ahmed *et al.,* 2020). Since oligomers are the primary neurotoxic species, and given that the E46K and A53T single point mutations cause PD onset decades earlier than normal, it is particularly interesting to speculate whether the enhanced interaction between ATP and, in particular, E46K αS could be related to an increased formation of toxic oligomers in younger individuals with familial PD that then causes the early disease onset (Ahmed *et al.,* 2020; Stephens *et al.,* 2020). In addition, the slight shifts in size of these disease-relevant αS oligomers by ATP could indicate structural rearrangements that have been shown to

mediate oligomer toxicity (Figure 8e) (Fusco *et al.,* 2017). In particular, the very significant increase in ThT-binding, β-sheet-rich E46K αS species with ATP addition could be reporting on an ATP-induced shift of E46K αS oligomers towards structures with higher β-sheet content, which has been associated with significantly increased toxicity (Figure 8d) (Fusco *et al.,* 2017). This hypothesis is further supported by the results in Figure 8b, which show that ATP addition increases the dynamics at the N- and C-termini of E46K αS monomers. Similarly dynamic N- and C-termini have been shown to be unique to more toxic αS species (Fusco *et al.,* 2017). By contrast, ATP in the presence of A53T αS does not cause an increase in ThT fluorescence despite still causing an increase in intermediately-sized, soluble αS species (Figure 8d and e). Thus, the ATP-induced size shift of these species could be due to a remodeling towards oligomers not sensitive to ThT (Figure 8d and e) (Fusco *et al.,* 2017). Thus, it is possible that ATP affects E46K and A53T αS by distinct mechanisms, both possibly leading to an alteration of PD-relevant oligomer cytotoxicity.

4.4 References for Chapters 3 and 4 Results and Discussion Sections

Ahmed, R., VanSchouwen, B., Jafari, N., Ni, X., Ortega, J., and Melacini, G. (2017) Molecular mechanism for the (−)-epigallocatechin gallate-induced toxic to nontoxic remodeling of aβ oligomers. *J. Am. Chem. Soc. 139,* 13720-13734.

Alza, N.P., Iglesias González, P.A., Conde, M.A., Uranga, R.M., and Salvador, G.A. (2019) Lipids at the crossroad of α-synuclein function and dysfunction: biological and pathological implications. *Front. Cell. Neurosci. 13,* doi: 10.3389/fncel.2019.00175.

Bisi, N., Feni, L., Peqini, K., Pérez-Peña, H., Ongeri, S., Pieraccini, S., and Pellegrino, S. (2021) α-synuclein: an all-inclusive trip around its structure, influencing factors and applied techniques. *Front. Chem. 9,* 666585.

Calamai, M., Kumita, J.R., Mifsud, J., Parrini, C., Ramazzotti, M., Ramponi, G., Taddei, N., Chiti, F., and Dobson, C.M. (2006) Nature and significance of the interactions between amyloid fibrils and biological polyelectrolytes. *Biochemistry. 45,* 12806-12815.

Chaudhari, S.N., and Kipreos, E.T. (2018) The energy maintenance theory of aging: maintaining energy metabolism to allow longevity. *Bioessays. 40,* e1800005.

Dang, M., Kang, J., Lim, L., Li, Y., Wang, L., and Song, J. (2021) ATP is a cryptic binder of TDP-43 RRM domains to enhance stability and inhibit ALS/AD-associated fibrillation. *Biochem. Bioph. Res. Co. 522,* 247-253.

Dettmer, U., Newman, A.J., von Saucken, V.E., Bartels, T., and Selkoe, D. (2015) KTKEGV repeat motifs are key mediators of normal α-synuclein tetramerization: their mutation causes excess monomers and neurotoxicity. *PNAS. 112,* 9596-9601.

Fusco, G., Chen, S.W., Williamson, P.T.F., Cascella, R., Perni, M., Jarvis, J.A., Cecchi, C., Vendruscolo, M., Chiti, F., Cremades, N., Ying, L., Dobson, C.M., and De Simone, A. (2017) Structural basis of membrane disruption and cellular toxicity by α-synuclein oligomers. *Science. 358,* 1440-1443.

Golts, N., Snyder, H., Frasier, M., Theisler, C., Choi, P., and Wolozin, B. (2002) Magnesium inhibits spontaneous and iron-induced aggregation of α-synuclein. *J. Biol. Chem. 277,* 16116-16123.

Greiner, J.V., and Glonek, T. (2020) Hydrotropic function of ATP in the crystalline lens. *Exp. Eye. Res. 190,* 107862.

Heo, C.E., Han, J.Y., Lim, S., Lee, J., Im, D., Lee, M.J., Kim, Y.K., and Kim, H.I. (2020) ATP kinetically modulates pathogenic tau fibrillations. *ACS. Chem. Neurosci. 11,* 3144-3152.

He, Y., Kang, J., and Song, J. (2020) ATP antagonizes the crowding-induced destabilization of the human eye-lens protein γS-crystallin. *Biochem. Biophys. Res. Commun. 526,* 1112-1117.

Holm, N.G. (2012) The significance of Mg in prebiotic geochemistry. *Geobiology. 10,* 269-279.

Lautenschläger, J., Stephens, A.D., Fusco, G., Ströhl, F., Curry, N., Zacharopoulou, M., Michel, C.H., Laine, R., Nespovitaya, N., Fantham, M., Pinotsi, D., Zago, W., Fraser, P., Tandon, A., St. George-Hyslop, P., Rees, E., Phillips, J.J., De Simone, A., Kaminski, C.F., and Kaminski Schierle, G.S. (2018) C-terminal calcium binding of α-synuclein modulates synaptic vesicle interaction. *Nat. Commun. 9,* 712.

Kang, J., Lim, L., and Song, J. (2018) ATP enhances at low concentrations but dissolves at high concentrations liquid-liquid phase separation (LLPS) of ALS/FTD-causing FUS. *Biochem. Bioph. Res. Co. 504,* 545-551.

Karamanos, T.K., Kalverda, A.P., Thompson, G.S., and Radford, S.E. (2015) Mechanisms of amyloid formation revealed by solution NMR. *Prog. Nucl. Mag. Res. Sp. 88-89,* 86-104.

Kumari, P., Ghosh, D., Vanas, A., Fleischmann, Y., Wiegand, T., Jeschke, G., Riek, R., and Eichmann, C. (2021) Structural insights into α-synuclein monomer–fibril interactions. *PNAS. 118,* e2012171118.

Lempart, J., Tse, E., Lauer, J.A., Ivanova, M.I., Sutter, A., Yoo, N., Huettemann, P., Southworth, D., and Jakob, U. (2019) Mechanistic insights into the protective roles of polyphosphate against amyloid cytotoxicity. *Life. Sci. Alliance. 2,* e201900486.

Moons, R., Konijnenberg, A., Mensch, C., Van Elzen, R., Johannessen, C., Maudsley, S., Lambeir, A-M., and Sobott, F. (2020) Metal ions shape α-synuclein. *Sci. Rep. 10,* 16293.

Nishizawa, M., Walinda, E., Morimoto, D., Kohn, B., Scheler, U., Shirakawa, M., and Sugase, K. (2021) Effects of weak nonspecific interactions with ATP on proteins. *J. Am. Chem. Soc. 143,* 11982-11993.

Reeve, A., Simcox, E., and Turnbull, D. (2014) Ageing and parkinson's disease: Why is advancing age the biggest risk factor? *Ageing. Res. Rev. 14,* 19-30.

Song, J. (2021) Adenosine triphosphate energy-independently controls protein homeostasis with unique structure and diverse mechanisms. *Protein. Sci. 30,* 1277-1293.

Stephens, A.D., Zacharopoulou, M., Moons, R., Fusco, G., Seetaloo, N., Chiki, A., Woodhams, P., Mela, I., Lashuel, H.A., Phillips, J.J., De Simone, A., Sobott, F., and Kaminski Schierle, G.S. (2020) Extent of N-terminus exposure of monomeric alpha-synuclein determines its aggregation propensity. *Nat. Commun. 11,* 1-15.

Yamaguchi, K., So, M., Aguirre, C., Ikenaka, K., Mochizuki, H., Kawata, Y., and Goto, Y. (2021) Polyphosphates induce amyloid fibril formation of α-synuclein in concentration-dependent distinct manners. *J. Biol. Chem. 296,* 100510.

Yamanaka, R., Tabata, S., Shindo, Y., Hotta, K., Suzuki, K., Soga, T., and Oka, K. (2016) Mitochondrial Mg^{2+} homeostasis decides cellular energy metabolism and vulnerability to stress. *Sci. Rep. 6,* 30027.

Zhang, N., An, L., Li, J., Liu, Z., and Yao, L. (2017) Quinary interactions weaken the electric field generated by protein side-chain charges in the cell-like environment. *J. Am. Chem. Soc. 139,* 647-654.

Chapter 5

Conclusions and Future Directions

5.1 Conclusion of the study

In this thesis, we established that the interaction between ATP and αS monomers is predominantly electrostatic and is driven most strongly by the phosphate groups targeting polar threonines and positively-charged lysine residues in the N-terminal "KTKEGV" protein repeats. Using primarily NMR-based chemical shifts, we found a complex dual system of Mg^{2+} sequestration from αS by ATP and *vice versa*. We found that ATP-Mg binds αS more weakly and that ATP is nonetheless unable to chelate 100% of equimolar Mg^{2+}, leaving a residual amount available to bind to and affect αS. The ATP-αS interaction, though relatively weak (K_d ~ mM), was found to be strong enough to disrupt long-range N- to C-terminal electrostatic contacts in αS monomers in a phosphate-dependent manner to enhance initial aggregation. Both ATP and ATP-Mg were found to significantly affect fibril formation, although in different ways, and we hypothesized that the significant inhibition of αS late-stage β-sheet fibril formation by ATP is likely, at least in part, to be due to ATP reducing electrostatically-driven αS monomer-fibril interactions and secondary nucleation. Finally, we found the effect of ATP to be significantly different in the presence of PD-related αS point mutations E46K and A53T. Unlike for WT, ATP increased the relative amounts of intermediately-sized, soluble E46K and A53T αS aggregates whilst having different effects on plateau β-sheet fibril formation compared to WT. Overall, our data indicate that ATP is indeed a "non-classical" hydrotrope with a dual effect on WT αS aggregation that is influenced by PD-relevant αS mutations.

5.2 Future Characterization of How ATP Affects Early Aggregate Formation of WT, E46K and A53T αS

In this thesis, we sought to characterize the overall effect of ATP on αS aggregation. Now, with the knowledge that ATP does indeed modulate the formation of early-stage αS aggregates, a critical next step becomes characterizing exactly how ATP influences initial αS monomer-monomer interactions and the formation of the first aggregation-competent primary nuclei since these species initiate cytotoxic oligomer formation and serve as templates for pathologically-relevant fibril strains (Ahmed *et al.,* 2020; de Oliveira and Silva, 2019). To begin addressing these questions, intermolecular PREs of ATP and all three αS variants should be performed to elucidate whether the ATP-driven NAC-region intensity changes in Figure 4b and 7b are due to increased self-association of NAC regions from multiple monomers. Concurrently, SEC-MALS, DLS and Circular Dichroism (CD) spectroscopy measurements should be performed throughout a time-course of concentration-dependent, ATP-induced αS aggregation similar to Figure 4c to monitor changes in monomer secondary structures and couple these to changes in the relative amounts of early αS aggregates. Hydrogen-deuterium exchange of these samples would also monitor the appearance of the fibril core (Cho *et al.,* 2011). In addition, for the PD-related E46K and A53T αS variants in particular, monitoring the time-course of concentration-dependent, ATP-induced aggregation via ThT would also establish whether the effects of ATP on E46K and A53T αS plateau fluorescence are coupled to an ATP-dependent enhancement of initial aggregation, as is the case for WT. It is interesting and pathologically-relevant to speculate whether the E46K and A53T αS mutations remove the bi-phasic effect of ATP on early- and late-stage WT αS aggregation

and whether or not a concentration-dependent enhancement of E46K and A53T oligomer formation explains the higher relative amounts of soluble, intermediately-sized αS aggregates in Figure 8e. Finally, to connect ATP-monomer interactions to ATP's effects on E46K and A53T αS aggregation, binding isotherms similar to those in Figure 2f should be created to confirm that the presence of additional lysine and threonine residues promotes enhanced binding between ATP and αS mutants. Intramolecular PREs of ATP and A53T αS monomers would also help elucidate if the intensity losses in Figure 8b report on threonine-driven increased αS monomer unfolding. This would explain the increase in soluble A53T aggregates by ATP. Overall, these results would help connect the residue-specific effects of ATP on αS monomers to early-aggregate formation and fully characterize the ATP-αS interactions that are likely to occur in early stages of PD development.

5.3 Future In-Depth Analysis of How ATP Exerts its Effect on αS Late-Stage Fibril Formation

We know from our ThT and TEM results at plateau that ATP decreases the formation of WT αS β-sheet-rich fibrils in a phosphate-dependent manner. However, we cannot conclude from this data alone whether the different effects of AMP versus ADP and ATP on plateau ThT fluorescence are a direct result of phosphate-dependent inhibition of αS secondary nucleation. Thus, residue-specific transverse ^{15}N αS R_2 amide relaxation experiments of WT αS monomers in the presence of fibrils and either AMP or ADP should be performed to characterize the effect of these ATP analogs on the N-terminal R_2 increases that indicate αS monomer-fibril interactions. If these data parallel

the plateau ThT results and show that ADP, but not AMP, attenuates the fibril-induced N-terminal R_2 increases, it would suggest that the varying effects of AMP, ADP and ATP on αS β-sheet fibril formation are due to a phosphate-dependent modulation of secondary nucleation. However, to further support the effect of ATP on αS secondary nucleation, ThT experiments should be performed with AMP, ADP and ATP in the presence of preformed fibrils, since these conditions favor monomer-fibril interactions and secondary nucleation over primary nucleus formation (Kumari *et al.,* 2021). Fully characterizing exactly how ATP attenuates αS monomer-fibril interactions could also provide a template for future development of therapeutic small molecules to inhibit seeding of PD pathology in patients.

Furthermore, a concentration-dependent addition of ATP to preformed WT αS fibrils and subsequent analysis by filtration and SDS-PAGE would also indicate whether ATP dissolves full-length αS fibrils, thereby providing another possible explanation for why ATP enhances initial αS aggregation but also decreases plateau ThT fluorescence. Performing these experiments in the presence of 150 mM NaCl and Mg^{2+} would also confirm that the ATP-driven effect on αS monomer-fibril interactions is indeed electrostatic and therefore modulated by biologically- and pathologically-relevant factors like Mg^{2+} complexation with ATP.

5.4 ATP as a Modulator of Oligomer-Induced WT, E46K and A53T αS Cytotoxicity

A fundamental open question generated by our findings is whether or not ATP's modulation of the relative amounts of intermediately-sized, soluble αS aggregates also influences their structure, and therefore, their PD-relevant cytotoxicity (Ahmed *et al.,*

2020; Fusco *et al.,* 2017). As a first step towards answering this question, STD-based binding isotherms similar to those in Figure 4f should be constructed using ATP and both monomers and oligomers of E46K and A53T αS. This would help determine whether the increase in the relative amounts of intermediate-sized E46K and A53T αS aggregates by ATP could be due to preferential oligomer vs. monomer ATP-binding, as is the case for WT (Figure 4f and 7e). In addition, the slight shifts in average size of the intermediate A53T and E46K αS aggregates by ATP could suggest structural rearrangements (Figure 8e). Therefore, CD of the soluble αS species formed at plateau should be performed to elucidate whether ATP causes changes in oligomer secondary structure since increases in β-sheet-content are correlated with αS oligomer toxicity (Fusco *et al.,* 2017). In addition, CD of WT, E46K and A53T αS monomers in both the absence and presence of ATP should be performed to characterize whether the targeting of N-terminal threonines within the “KTK” repeats by ATP influences their α-helical content (Dettmer *et al.,* 2015). This could also provide an indication of ATP’s influence on cytotoxicity, which typically helical tetramers reduce (Dettmer *et al.,* 2015). To connect these potential differences in α-helical- and β-sheet-content to cytotoxicity, Presto Blue cell viability assays should be performed using the isolated, soluble αS WT, E46K, and A53T aggregates formed at plateau in both the absence and presence of ATP (Ahmed *et al.,* 2020). Altogether, these experiments would characterize a potential mechanism whereby ATP modulates PD-relevant neurotoxicity and could explain the early-onset neurodegeneration in E46K and A53T-associated familial PD cases as a function of ATP-induced toxic αS oligomer formation (Stephens *et al.,* 2020).

5.5 The Potential Biological Role of ATP in Controlling αS Monomer-Lipid Interactions

Given that ATP preferentially targets the N-terminal "KTKEGV" pseudo-apolipoprotein-like repeats in αS monomers that confer the protein's lipid-binding properties, our research suggests that ATP could modulate the biologically-relevant interaction between αS and membranes (Alza *et al.,* 2019). Specifically, since αS-membrane interactions are predominantly electrostatic and preferentially involve negatively-charged lipids which associate with positive lysines in the αS N-terminus, it is likely that the N-terminal binding and positive-charge-neutralization of αS monomers by ATP reduces protein-membrane binding (Bozelli Jr. *et al.,* 2021). To explore this hypothesis, NMR-based binding experiments involving αS and lipid vesicles that resemble neuronal membranes should be performed in the presence of increasing concentrations of ATP, ATP analogs, and Mg^{2+} to elucidate whether the residue-specific αS chemical shifts and R_2 amide relaxation parameters caused by lipid binding are affected in a phosphate-dependent manner by ATP addition. Furthermore, ThT-based experiments monitoring αS aggregation in the presence of ATP and lipid vesicles should be performed to characterize whether the aggregation-promoting effect of membranes on αS is attenuated by ATP (Bozelli Jr. *et al.,* 2021). To validate these experiments using other more traditional methods of monitoring protein-lipid interactions, we could also perform co-sedimentation assays as well as fluorescence spectroscopy or fluorescence resonance energy transfer experiments using αS, ATP and lipid vesicles (Zhao and Lappalainen, 2012). If these experiments do indeed show that ATP binding to αS influences the protein's ability to interact with membranes, it would suggest a new role for

ATP in modulating the biological function of αS in synaptic vesicle trafficking by selectively binding or interfering with lipid membranes (Bozelli Jr. *et al.,* 2021).

5.6 The Pathological Effect of ATP on αS Aggregation Could Involve Modulating LLPS

Having established that ATP interacts primarily with the N-terminus of αS monomers to enhance initial aggregation, a logical hypothesis is that ATP likely also modulates αS LLPS, which is driven by the N-terminus and which nucleates αS aggregation (Ray *et al.,* 2020). The bi-phasic effect of ATP on αS aggregation certainly resembles the concentration-dependent modulation of FUS LLPS by ATP and is likewise driven in large part by the triphosphate moiety interacting with protein lysine residues (Kang *et al.,* 2018). In addition, factors which affect αS aggregation, such as low pH as well as the presence of metal ions and liposomes, also affect αS LLPS (Ray *et al.,* 2020). Therefore, it is not unreasonable to assume that the same may be true for ATP. Finally, since interdomain interactions likely drive αS LLPS and we show that ATP disrupts such long-range N- to C-terminal domain contacts, it is particularly interesting to speculate whether the enhancement of initial αS aggregation by ATP is accompanied by an ATP-dependent decrease or increase in αS LLPS, both of which have pathological implications (Ray *et al.,* 2020). Therefore, to address this hypothesis, a time-course of fluorescently-labelled αS aggregation in the presence of ATP, ATP analogs and Mg^{2+} should be performed and droplet formation should be monitored by fluorescence microscopy and TEM. Finally, to connect the potential effect of ATP on αS LLPS to its effect on aggregation, the dynamics of proteins within the LLPS droplets should be monitored by

fluorescence recovery after photobleaching (FRAP) experiments (Ray *et al.,* 2020). By performing these experiments, we would hope to characterize an additional mechanism by which ATP modulates pathologically-relevant αS aggregation by controlling aggregation-nucleating LLPS (Ray *et al.,* 2020).

5.7 References

Ahmed, R., Huang, J., Weber, D.K., Gopinath, T., Veglia, G., Akimoto, M., Khondker, A., Rheinstädter, M.C., Huynh, V., Wylie, R.G., Bozelli Jr., J.C., Epand, R.M., and Melacini, G. (2020) Molecular mechanism for the suppression of alpha synuclein membrane toxicity by an unconventional extracellular chaperone. *J. Am. Chem. Soc. 142,* 9686-9699.

Alza, N.P., Iglesias González, P.A., Conde, M.A., Uranga, R.M., and Salvador, G.A. (2019) Lipids at the crossroad of α-synuclein function and dysfunction: biological and pathological implications. *Front. Cell. Neurosci. 13,* doi: 10.3389/fncel.2019.00175.

Bozelli Jr., J.C., Kamski-Hennekam, E., Melacini, G., and Epand, R.M. (2021) α-Synuclein and neuronal membranes: Conformational flexibilities in health and disease. *Chem. Phys. Lipids. 235,* 105034.

Cho, M-K., Kim, H-Y., Fernandez, C.O., Becker, S., and Zweckstetter, M. (2011) Conserved core of amyloid fibrils of wild type and A30P mutant α-synuclein. *Protein. Sci. 20,* 387-395.

de Oliveira, G.A.P., and Silva, J.L. (2019) Alpha-synuclein stepwise aggregation reveals features of an early onset mutation in parkinson's disease. *Commun. Biol. 2,* 374.

Dettmer, U., Newman, A.J., von Saucken, V.E., Bartels, T., and Selkoe, D. (2015) KTKEGV repeat motifs are key mediators of normal α-synuclein tetramerization: their mutation causes excess monomers and neurotoxicity. *PNAS. 112,* 9596-9601.

Fusco, G., Chen, S.W., Williamson, P.T.F., Cascella, R., Perni, M., Jarvis, J.A., Cecchi, C., Vendruscolo, M., Chiti, F., Cremades, N., Ying, L., Dobson, C.M., and De Simone, A. (2017) Structural basis of membrane disruption and cellular toxicity by α-synuclein oligomers. *Science. 358,* 1440-1443.

Kang, J., Lim, L., and Song, J. (2018) ATP enhances at low concentrations but dissolves at high concentrations liquid-liquid phase separation (LLPS) of ALS/FTD-causing FUS. *Biochem. Bioph. Res. Co. 504,* 545-551.

Kumari, P., Ghosh, D., Vanas, A., Fleischmann, Y., Wiegand, T., Jeschke, G., Riek, R., and Eichmann, C. (2021) Structural insights into α-synuclein monomer–fibril interactions. *PNAS. 118,* e2012171118.

Ray, S., Singh, N., Kumar, R., Patel, K., Pandey, S., Datta, D., Mahato, J., Panigrahi, R., Navalkar, A., Mehra, S., Gadhe, L., Chatterjee, D., Sawner, A.S., Maiti, S., Bhatia, S., Gerez, J.A., Chowdhury, A., Kumar, A., Padinhateeri, R., Riek, R., Krishnamoorthy, G.,

and Maji, S.K. (2020) α-Synuclein aggregation nucleates through liquid–liquid phase separation. *Nat. Chem. 12,* 705-716.

Stephens, A.D., Zacharopoulou, M., Moons, R., Fusco, G., Seetaloo, N., Chiki, A., Woodhams, P., Mela, I., Lashuel, H.A., Phillips, J.J., De Simone, A., Sobott, F., and Kaminski Schierle, G.S. (2020) Extent of N-terminus exposure of monomeric alpha-synuclein determines its aggregation propensity. *Nat. Commun. 11,* 1-15.

Zhao, H., and Lappalainen, P. (2012) A simple guide to biochemical approaches for analyzing protein–lipid interactions. *Mol. Biol. Cell. 23,* 2823-2830.

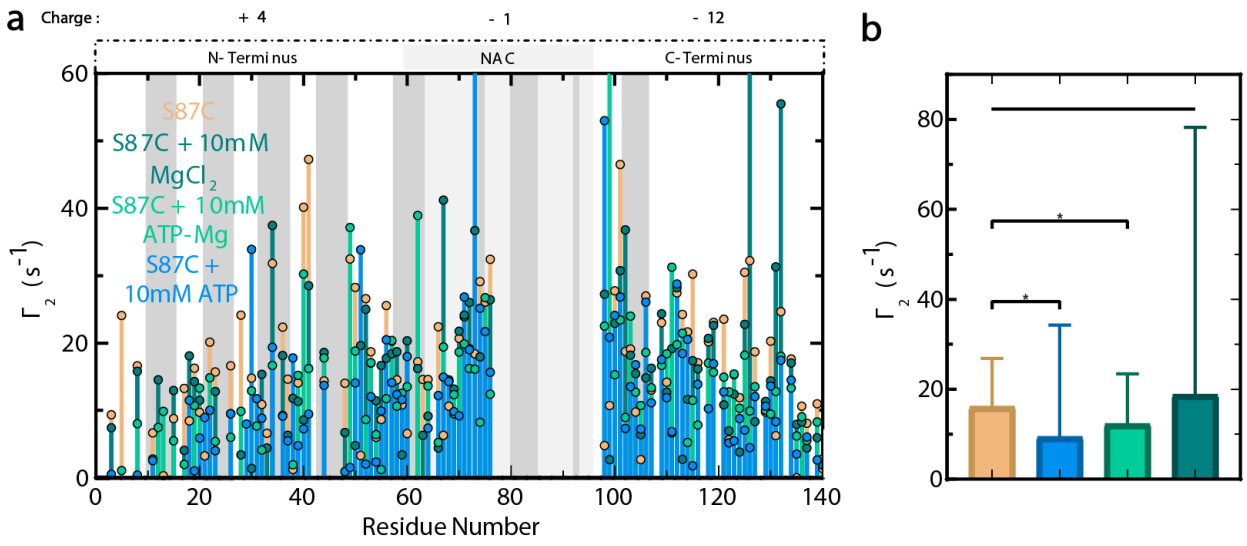

Supplementary Figure 1. Magnesium partially attenuates the ATP-mediated disruption of long-range interactions in αS monomers. (a) Residue-specific Γ_2 values for spin-labeled, fresh 120 µM S87C ^{15}N αS in the absence (brown) or presence of 10 mM ATP, ATP-Mg or $MgCl_2$. (b) Average and standard deviation of all residues for each condition in panel a combined, colored as per legend in a and compared using an unpaired t-test with a flat line without * representing no significant difference and * representing $0.01 < p < 0$. For panel a, the 10 residues on either side of residue 87 are not shown, and the charges of each labelled αS region are shown above the plots with the dark grey boxes representing the imperfect "KTKEGV" αS repeats. Residues with significant overlap or for which peaks entirely disappeared in one or more conditions are not shown. All NMR experiments were performed using αS in 50 mM Hepes, 5% D_20, pH 7.4 buffer on a Bruker AV 700 spectrometer at 10 ºC. All figures were prepared in GraphPad Prism 8.4.2. and Adobe Illustrator 26.3.1.

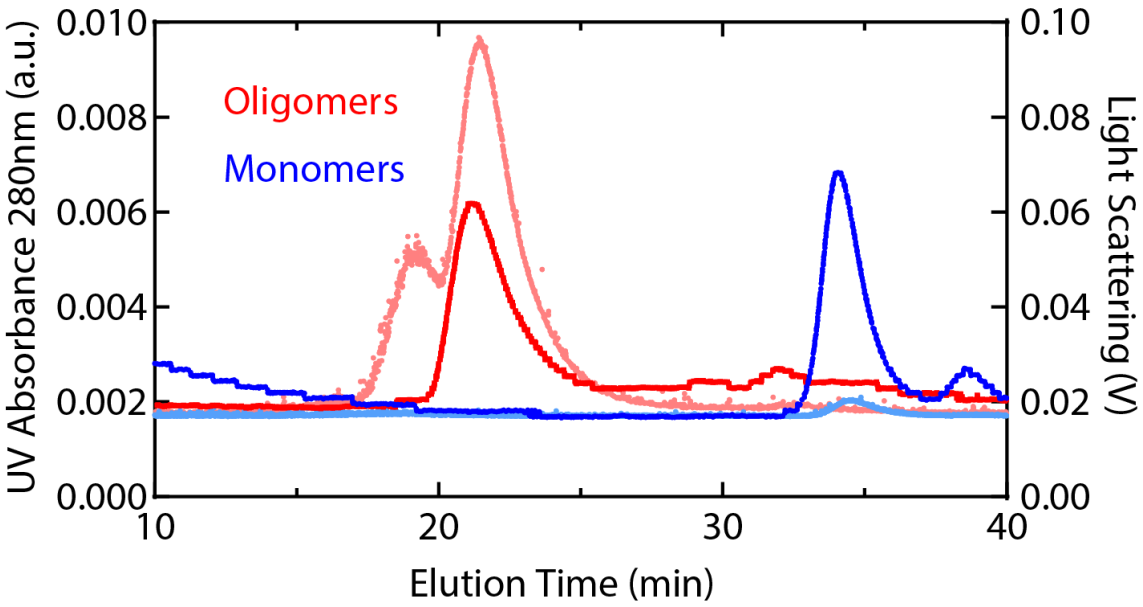

Supplementary Figure 2. SEC-MALS characterization of αS monomers and oligomers. UV absorbance and light scattering measurements of αS monomers (blue) as well as oligomers (red) used for 1D STD experiments, characterized by Size Exclusion Chromatography Coupled with Multiangle Light Scattering (SEC-MALS). UV absorbance and light scattering measurements are shown in darker and lighter color tones, respectively, and are plotted relative to elution time. Figure prepared in GraphPad Prism 8.4.2. and Adobe Illustrator 26.3.1.

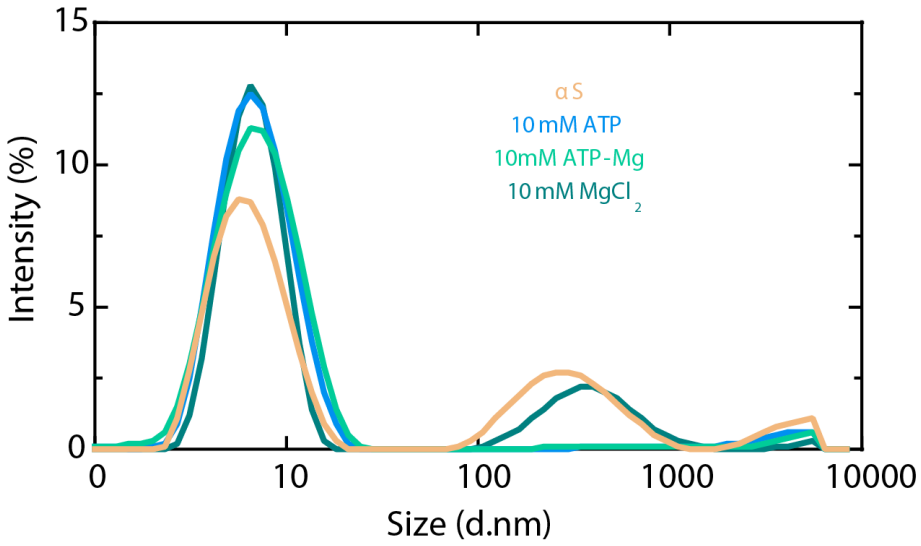

Supplementary Figure 3. ATP suppresses the formation of intermediate-size, soluble αS aggregates in both the absence and presence of magnesium. Dynamic Light Scattering (DLS) intensity measurements of soluble αS recovered from specific samples from Figure 5, panel (a) at plateau and following centrifugation to pellet large aggregates. Figure prepared in GraphPad Prism 8.4.2. and Adobe Illustrator 26.3.1.